Desalination 292 (2012) 87–104

Contents lists available at SciVerse ScienceDirect

Desalination

journal homepage: www.elsevier.com/locate/desal

Modeling and genetic algorithm-based multi-objective optimization of the MED-TVC desalination system

Iman Janghorban Esfahani [a], Abtin Ataei [b], Vidya Shetty K [c,*], TaeSuk Oh [a], Jae Hyung Park [d,*], ChangKyoo Yoo [a,*]

[a] Department of Environmental Science & Engineering, Green Energy Center/Center for Environmental Studies, Kyung Hee University, Seocheon-dong 1, Giheung-gu. Yongin-Si, Gyeonggi-Do 446-701, Republic of Korea
[b] Department of Energy Engineering, Graduate School of the Environment and Energy, Science and Research Branch, Islamic Azad University, Tehran, Iran
[c] Department of Chemical Engineering, National Institute of Technology Karnataka Surathkal, Srinivasnagar, India
[d] Department of Polymer Science and Engineering, Sungkyunkwan University, Suwon 440-746, Republic of Korea

ARTICLE INFO

Article history:
Received 31 October 2011
Received in revised form 12 February 2012
Accepted 13 February 2012
Available online 8 March 2012

Keywords:
Desalination
Economic costs
MED-TVC
Mathematical modeling
Artificial neural network
Multi-objective optimization

ABSTRACT

This study proposes a systematic approach of analysis and optimization of the multi-effect distillation-thermal vapor compression (MED-TVC) desalination system. The effect of input variables, such as temperature difference, motive steam mass flow rate, and preheated feed water temperature was investigated using response surface methodology (RSM) and partial least squares (PLS) technique. Mathematical and economical models with exergy analysis were used for total annual cost (TAC), gain output ratio (GOR) and fresh water flow rate (Q). Multi-objective optimization (MOO) to minimize TAC and maximize GOR and Q was performed using a genetic algorithm (GA) based on an artificial neural network (ANN) model. Best Pareto optimal solution selected from the Pareto sets showed that the MED-TVC system with 6 effects is the best system among the systems with 3, 4, 5 and 6 effects, which has a minimum value of unit product cost (UPC) and maximum values of GOR and Q. The system with 6 effects under the optimum operation conditions can save 14%, 12.5%, 2% in cost and reduces the amount of steam used for the production of 1 m^3 of fresh water by 50%, 34% and 18% as compared to systems with 3, 4 and 5 effects, respectively.

1. Introduction

Due to the rapid growth of population, industry, and irrigation during the second half of the last century, the need for high-quality water has significantly increased. Desalination technologies have been greatly improved in the last few decades in order to produce potable water. Today, thermal desalination processes account for more than 65% of the production capacity of the desalination industry [1,2].

Among thermal desalination systems, multi-effect distillation-thermal vapor compression (MED-TVC) systems with a top brine temperature (TBT) lower than 70 (°C) have received more attention in recent years [3]. In these systems, a steam jet ejector is added to a multi-effect distillation (MED) system to reduce the amount of required steam (motive steam), boiler size, and the amount of cooling water, thereby lower pumping power and pretreatment costs [4]. Expansion in desalination systems is associated with an increase of the gain output ratio (GOR) and a decrease in total annual cost (TAC), with the maximum production of fresh water (Q).

Recently, several studies have been carried out on the modeling and single-optimization of MED-TVC systems. Bin Amer [5] optimized the ME-TVC system using Smart Exhaustive Search Method and Sequential Quadratic Programming. Bin Amer [5] approach was applied to maximize the GOR of the MED-TVC system. Kamali et al. [2], El-Dessouky et al. [6], Zhao et al. [7], Alasfour et al. [1], and Al-Salahi and Ettouney [8]have developed steady state mathematical models to represent a MED-TVC desalination system and parametric techniques have been used to determine the optimum operating and design conditions for the system. Sayyaadi et al. [18] performed thermodynamic and thermoeconomic optimization of MED-TVC using a hybrid stochastic/deterministic optimization approach based on a combination of GA and simulated annealing (GA + SA). All of mentioned papers focused on the single-optimization approach. Shakouri et al. [3], Lukic et al. [9], Choi et al. [10], Ansari et al. [11], and Sharaf et al. [12] have developed mathematical and economic models for a MED-TVC system and performed the exergy analysis. Shakouri et al. [3] optimized MED-TVC system based on minimization of unit product cost. In the Shakouri et al's [3] exergy analysis approach, the exergy destruction was considered as a new term to operating cost. Choi et al. [10] evaluated the exergy losses due to irreversibility in each subsystems of MED-TVC desalination system and identified the potential for improving system efficiency using exergy analysis.

* Corresponding authors.
E-mail addresses: vidyaks68@yahoo.com, vidyaks95@nitk.ac.in (V. Shetty K), jhpark1@skku.edu (J.H. Park), ckyoo@khu.ac.kr (C.K. Yoo).

0011-9164/$ – see front matter © 2012 Elsevier B.V. All rights reserved.
doi:10.1016/j.desal.2012.02.012

Recently, several studies have been performed using MOO to optimize desalination systems. Vince et al. [15] have carried out MOO to minimize the electrical consumption and total water price in RO network using mixed integer nonlinear programming. Guria et al. [16] applied MOO to minimize the permeate throughput, the cost of desalination, and the permeate concentration of reverse osmosis desalination units using different adaptations of the non-dominated (NSGA). Khoshgoftar Manesh and Amidpour [17] applied an evolutionary algorithm to multi-objective thermoeconomic optimization of coupling a multi stage flash desalination (MSF) plant with a pressurized water reactor (PWR) nuclear power plant.

For MOO problems, a set of optimal solutions called the Pareto front exists, corresponding to a set of input decision variables. According to the required conditions, designers can choose a set of design variables (input decision variables) to design an optimal system using the Pareto front. Recently, genetic algorithms (GA) have been efficiently used for solving multi-objective optimization problems in engineering. GA is a globally heuristic, stochastic optimization technique based on the theory of evolution [13,14].

Mathematical models of the process, which present the objective functions correlated to the decision variables, are needed for MOO. Since the theoretical models of MED-TVC systems are complex and cannot be easily implemented in MOO using GA, an artificial neural network (ANN) based model of a MED-TVC system is proposed in the present study. ANN, as the branch of artificial intelligence, is a powerful tool to model complex non-linear systems [19]. ANN models have been developed in the current study, using the theoretical model simulation results for the input conditions, based on the design of experiments (DOE) methodology. ANN models have been applied earlier in order to optimize desalination systems, but were not used for MED-TVC systems.

In order to understand the contribution of each of the decision variables individually and their interaction effects, response surface methodology (RSM) is applied to the MED-TVC system. Khayet et al. [20] and Kazemian et al. [21] have optimized and investigated both RO and thermal desalination systems, using RSM.

To evaluate the correlation between the output variables (responses) and input variables, partial least squares (PLS) is used. PLS is a hybrid method of multiple regression and Principal Component Analysis (PCA) [25].

As were investigated in the literature, recent research efforts have been focused on a formal mathematical approach to provide a clear evaluation and single objective optimization of the MED-TVC desalination system. However, studies on the multi-objective optimization (MOO) of MED-TVC systems in order to maximize GOR and minimize UPC, simultaneously, are scarce.

This paper contributes to a new approach to the optimization and investigation of MED-TVC desalination systems. MOO is applied to minimize TAC and maximize GOR and Q simultaneously, while the temperature difference between effects (ΔT), motive steam mass flow rate (S), and preheated seawater temperature (T_{ph}) are considered as the input decision variables.

By this approach, more details of the process are investigated using RSM and PLS modeling and MOO provides better decision-making tool based on the designer's requirements for MED-TVC optimal designing, which have not considered in resent research.

The objectives of this paper are summarized in five sections. First is choosing the set of input decision variable values based on central composite experimental design (CCD) and then determining output variables for these sets, using the mathematical and economical models of the process, respectively. Second is the use of exergy analysis to calculate the amount of exergy destruction as an opportunity cost. Third is the process of analyzing and investigating the effects of input variables on the responses of RSM and PLS. Fourth is developing the ANN model and optimizing the MED-TVC systems with different numbers of effects (n) by subjecting the ANN model to MOO, using GA in order to minimize TAC and maximize GOR and Q. This will also include the presentation of Pareto optimal solutions and the selection of two points as preferred points based on the minimization of unit product cost (UPC) and the maximization of GOR. The final section is the definition of the sets of input decision variables corresponding to preferred points as the design parameters.

2. Material and methods

2.1. MED-TVC configuration

The schematic of a MED-TVC system with 'n' effects is shown in Fig. 1. The system includes a steam jet ejector (SJE), evaporators, pre-heaters, flashing boxes and an end condenser. In the MED-TVC system, the motive steam is used by an SJE to compress some of the water vapor produced in the last effect. The compressed vapor is introduced into the tube side in the first effect and condensed by releasing its latent heat into the feed water for evaporation. Part of the condensate returns to the boiler, and other part passes into the first flashing box. Demisted vapor formed in the first effect and the flashed vapor from the first flashing box is used together as heating sources in the first preheater to preheat the feed water to the first effect. The combined vapor from the first pre-heater passes into the second effect and is used as the heat source to vaporize the feed water in the second effect. This process is repeated for all effects until the last one. At the end, the generated vapor of the last effect passes through

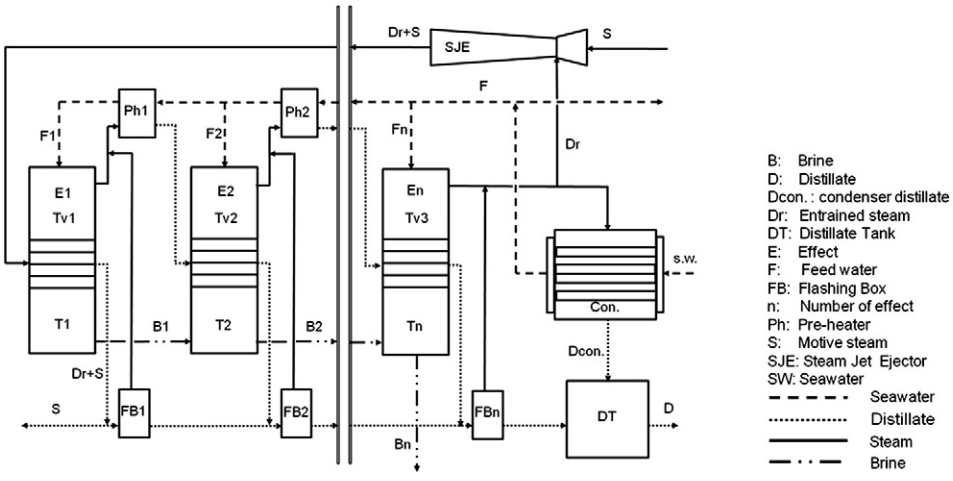

Fig. 1. Schematic of the MED-TVC system with n effects.

Table 1
Mass balance, GOR and Q equations.

Equations	Descriptions	
$B_1 = F_1 - D_1$	Mass balance of effect 1	(1)
$B_i = F_i + B_{i-1} - D_i + \left[y_{i-1}\cdot\left(D_r + \sum_{j=1}^{i-2} D_j\right)\right] - [(i-1).F_{i-1}.y_{i-1}]$	Mass balances of effects 2 to n	(2)
$D_{con.} = D_n - D_r + \left[y_n\cdot\left(D_r + \sum_{i=1}^{n-1} D_i\right)\right]$	Mass balance of end condenser	(3)
$D = \left[(1-y_n).\left(D_r + \sum_{i=1}^{n-1} D_i\right)\right] - \left[y_{n-1}\cdot\left(D_r + \sum_{i=1}^{n-2} D_i\right)\right] - \left[y_{n-2}\cdot\left(\sum_{i=1}^{n-3} D_i\right)\right] - \left[y_{n-3}\cdot\left(D_r + \sum_{i=1}^{n-4} D_i\right)\right] - \left[y_{n-4}\cdot\left(D_r + \sum_{i=1}^{n-5} D_i\right)\right] - (y_{n-5}.D_r) + D_{con}.y_6 \geq y \geq y_1$	Mass balance of distillate tank	(4)
$C_{sw}F_1 = C_{B1}B_1$	Salinity balance of effect 1	(5)
$C_{sw}F_i + (C_{B_{i-1}}.B_{i-1}) = C_{Bi}B_i$	Salinity balance of effects 2 to n	(6)
$GOR = \frac{D}{S}$	Gain output ratio	(7)
$Q = 86.4 \cdot D$	Fresh water flow rate	(8)

the condenser. The condensed vapor is introduced into the distillate tank and the cooling water is divided into two parts. The first part is used as feed and is distributed among the effects, and the other part is rejected back to the sea [3,5].

2.2. Theoretical modeling of a MED-TVC system

The MED-TVC system has been modeled in two parts. The first part is the phenomenological mathematical model for the process, and the second part is the economic model. The models developed by Alasfour et al.[1], Shakouri et al. [3], and Bin Amer [5] have been applied in the current study. In the phenomenological model development, the mass and energy balances and the heat transfer equations for evaporators, pre-heaters, jet ejectors, and end condensers have been developed. These model equations can be simulated to determine the values of GOR and Q. The economic model and the phenomenological mathematical model are used to obtain the TAC of the MED-TVC system. Exergy destruction has been considered as a new cost term, which is included in the operating cost in the economic model.

2.2.1. Phenomenological mathematical model

Several simplifying assumptions listed below [3,7] were used in the development of the phenomenological mathematical models:

- The plant is operated under a steady state.
- Heat losses to the surroundings are negligible.
- The temperature differences across the feed heaters are equal in order to achieve the optimum operating conditions.
- The feed flow rates in all the effects are equal.
- Distillated water (produced water in the nth effect) is free of salt (i.e. it has zero salinity).

Mass and salinity balance equations for all the effects, the condenser, and the distillate tank are given by Eqs. (1)–(6), as shown in Table 1. Energy balance equations for all the effects are given by Eqs. (9) and (10) that are presented in Table 2.

The heat transfer area for each effect, the pre-heaters, the condenser, and the total heat transfer area can be obtained by using Eqs. (11)–(16), as shown in Table 3. In addition, the overall heat transfer coefficients and the logarithmic mean temperature differences for the effects, pre-heaters, and condenser are given by Eqs. (17)–(24), as shown in Table 3.

The temperature profile equations to determine the saturated vapor temperature, vapor condensation temperature, brine temperature and non-equilibrium allowance are presented in Table 4. The thermodynamic parameters' initial circumstances are presented in Table 5.

2.2.2. Economic modeling

The total annual cost function is given by Eq. (31).

$$TAC = ACC + AOC \tag{31}$$

where ACC and AOC are the annual capital cost and annual operating cost, respectively. The economic model equations that are used to calculate the TAC are shown in Table 6. The annual capital cost (ACC) is obtained by multiplying capital cost by the amortization factor. The capital cost includes the area cost (C_A), instrument cost (C_{eq}), site cost (C_s), transportation cost (C_{tr}), building cost (C_b), engineers and salary cost (C_{en}), and contingency cost (C_c), which are given by Eqs. (32)–(39). The capital cost should be amortized to calculate the ACC. The amortization factor is given by Eq. (40), in which the interest rate (i) and plant life cycle (m) have been assumed to be equal to 15% and 20 years, respectively.

The AOC includes thermal energy cost (C_{th}), electricity cost (C_e), labor cost (C_l), chemical materials cost (C_{ch}), and insurance cost (C_{in}), which are calculated by Eqs. (42)–(46). Exergy destruction has been considered to be a lost opportunity cost term. This term is considered in operating cost. The amount of exergy destruction in the MED-TVC system is calculated by the application of equations that are given in Table 7 [3]. The cost of power is assigned based on the price of electricity being 0.07 ($/kWh). As the plant is assumed to operate 330 days a year, the plant load factor (f) is considered to be 0.9 [1,3,7].

Table 2
Energy balance equations.

Equations	Descriptions	
$D_1 \cdot L_1 + (F_1 \cdot Cp \cdot (T_1 - T_{f1})) = (Dr + S) \cdot L_0$	Energy balance of effect 1	(9)
$D_i \cdot L_i + (F_i \cdot Cp \cdot (T_i - T_{fi})) = (D_{i-1} \cdot L_{i-1}) + \left(y_{i-1} \cdot \left(D_r + \sum_{j=1}^{i-2} D_j\right) \cdot L_{i-1}\right) - ((i-1) \cdot F_{i-1} \cdot y_{i-1} \cdot L_{i-1}) + (B_{i-1} \cdot C \cdot (T_{i-1} - \bar{T}_i)$	Energy balance of effects 2 to n	(10)

Table 3
Heat transfer area, heat transfer coefficient, and logarithmic mean temperature difference equations.

Equations	Descriptions	
$A_{e1} = \frac{(Dr+S)\cdot L_0}{U_{e1}\cdot(T_{0C}-T_1)}$	Heat transfer area of effect 1	(11)
$A_{ej} = \frac{\left(\left(D_{i-1}+\left(\left(D_r+\sum_{j=1}^{i-2}D_j\right)\cdot y_{i-1}\right)-((i-1)\cdot y_{i-1}\cdot F_i)\right)\cdot L_{i-1}\right)}{U_{ei}\cdot(T_{v_{i-1}}-T_i)}$	Heat transfer area of effects 2 to n	(12)
$A_{tot} = \sum_{i=1}^{n} A_i$	Total heat transfer area of effects	(13)
$A_{H_i} = \frac{(i\cdot F_i\cdot C\cdot(T_{f_i}-T_{f_{i+1}}))}{U_{H_i}\cdot LMTD_{H_i}}$	Heat transfer area of pre-heaters 1 to n-1	(14)
$A_{H_n} = \frac{(n\cdot F_n\cdot(T_{f_n}-T_f))}{U_{H_n}\cdot LMTD_{H_n}}$	Heat transfer area of pre-heater n	(15)
$A_{con.} = \frac{\left(D_{con.}+\left(\left(D_r+\sum_{j=1}^{n-1}D_j\right)\cdot y_n\right)\right)\cdot L_n}{U_{con.}\cdot LMTD_{con.}}$	Heat transfer area of end condenser	(16)
$U_{e1} = 1.9394+(1.40562\times10^{-3})\cdot T_{0c}-(2.07525\times10^{-5})\cdot T_{0c}^2+(2.3186\times10^{-6})\cdot T_{0c}^3$	Heat transfer coefficient of effect 1	(17)
$U_{ei} = 1.9394+(1.40562\times10^{-3})\cdot T_{vi_{-1}}-(2.07525\times10^{-5})\cdot T_{vi_{-1}}{}^2+(2.3186\times10^{-6})\cdot T_{vi_{-1}}{}^3$	Heat transfer coefficient of effects 2 to n	(18)
$U_{H_i} = 14.18251642+0.011383865\cdot T_{v_i}+0.013381501\cdot T_{f_{i+1}}$	Heat transfer coefficient of pre-heaters 1 to n-2	(19)
$U_{H_{n-1}} = 14.18251642+0.011383865\cdot T_{v_{n-1}}+0.013381501\cdot T_f$	Heat transfer coefficient of pre-heaters n-1	(20)
$U_{con.} = 1.6175+(1.537\times10^{-4})\cdot T_{v_n}-(1.825\times10^{-4})\cdot T_{v_n}{}^2+(8.026\times10^{-8})\cdot T_{v_n}{}^3$	Heat transfer coefficient of end condenser	(21)
$LMTD_{H_i} = (T_{f_i}-T_{f_{i+1}})/\left(\ln\frac{T_{v_i}-T_{f_{i+1}}}{T_{v_i}-T_{f_i}}\right)$	Logarithmic mean temperature difference of effects 1 to n-2	(22)
$LMTD_{H_{n-1}} = (T_{f_{n-1}}-T_f)/\left(\ln\frac{T_{v_{n-1}}-T_f}{T_{v_{n-1}}-T_{f_{n-1}}}\right)$	Logarithmic mean temperature difference of effect n-1	(23)
$LMTD_{con.} = (T_f-T_{sw})/\left(\ln\frac{T_{v_n}-T_{sw}}{T_{v_n}-T_f}\right)$	Logarithmic mean temperature difference of end condenser	(24)

2.3. Response surface methodology (RSM) modeling

To determine optimum operation conditions and investigate the behavior the factors on the responses of the system, a model is used to create a valid of the experimental domain given by the significant factors and their ranges. The RSM consists of a group of mathematical and statistical techniques devoted to the evaluation of the relationship between the dependent variable or response (Y) and the set of independent variables or factors (X_1,.., X_k). RSM is used to determine the critical points (maximum, minimum, or saddle) of the response by finding the optimal settings of the factors as well as to analyze the effect of input variables on the response surfaces [22,23]. RSM can illustrate the response surface of the dependent variables by varying a number of independent variables or factors, which affect the responses of the dependant variables. RSM is less laborious and time-consuming than other approaches and is an effective technique for optimizing complex processes, since it reduces the number of experiments needed to evaluate multiple parameters and their interactions [38].

When it is assumed that the k number of independent variables, $X=(X_1, X_2,..., X_k)$, affects the p number of response variables, $Y=(Y_1,Y_2,...,Y_p)$, the general function oh the response surface method could be represented as Eq. (56).

$$Y_{ij} = f_i(X_1, X_2, ..., X_k), \quad , i = 1, 2, ..., p \quad and \quad j = 1, 2, ..., k \tag{56}$$

Table 4
Temperature profile equations.

Equations	Descriptions	
$T_i = T_{vi}+(BPE)_i+\Delta T_{yi}$	Saturated vapor temperature of effects	(25)
$T_{ci} = T_{vi}-(\Delta T_p)_i$	Vapor condensation temperature of effects	(26)
$T_1 = T_{0c}+NEA_1$	Flashing vapor condensation temperature of effect 1	(27)
$T_i = T_{vi}+NEA_i$	Flashing vapor condensation temperature of effects 2 to n	(28)
$T'_i = T_i+NEA_i$	Flashing brines temperature of effects 2 to n	(29)
$(NEA)_i = (0.33(T_{i-1}-T_i)^{0.55})/T_{vi}$	Non-equilibrium allowance	(30)

where f_i is a function between response variables and dependent variables. Because f_i is generally an unknown function, it is assumed that it can be calculated through experimentation [27].

The relationship between the response and the factors is explained by the second-order polynomial regression model shown in Eq. (57) [24].

$$Y = \beta_0 + \sum_{i=1}^{n}\beta_i x_i + \sum_{i=1}^{n}\beta_{ii}x_i^2 + \sum_{i=1}^{n-1}\sum_{j=1}^{n}\beta_{ij}x_i x_j \tag{57}$$

where Y is the response variable; x_i and x_j are the coded levels of the input variables; β_0 is the intercept term; and β_i, β_{ii}, and β_{ij} are the coefficients representing the linear effect, quadratic effect, and interaction effect, respectively, which are known as the regression coefficients.

The significance of input variables, their interactions, and the goodness of fit of the RSM models were tested by analysis of variance (ANOVA). An alpha (α) level of 0.05 was used to determine the statistical significance in all analysis. The significance of each of the coefficients was determined using F-values and P-values. The effect terms with coefficients having F-values greater than Fisher's F-test values and P-values less than 0.05 are considered to have high significance on the RSM models. Fisher's F-test is calculated by Eq. (58) using MATLAB software.

$$Fisher's\ F-test = F_{\alpha,df,(n-df+1)} \tag{58}$$

where α, df and n are desired probability level, degree of freedom and observations.

Table 5
Thermodynamic parameters' initial circumstances.

Discretion	Parameter	Unit	Value
Salinity of seawater	C_{sw}	ppm	36,000
Salinity of last effect brine	C_{bn}	ppm	70,000
Temperature of seawater	T_{sw}	°C	25
Pressure of seawater	P_{sw}	kpa	101
Top brine temperature	TBT	°C	69
Boiling point elevation	BPE	–	0.8

Table 6
Economic model equations.

Equations	Descriptions	
Capital costs		
$C_A = 140 \cdot A_E$	Area cost ($)	(32)
$C_{eq} = 4 \cdot C_A$	Instrument cost (evaporator, condenser…) ($)	(33)
$C_s = 0.2 \cdot C_{eq}$	Site cost ($)	(34)
$C_{tr} = 0.05 \cdot (C_A + C_{eq} + C_s)$	Transportation costs ($)	(35)
$C_b = 0.15 \cdot C_{eq}$	Building costs ($)	(36)
$C_{en} = 0.1 \cdot C_{eq}$	Engineers and salary costs ($)	(37)
$C_c = 0.1 \cdot (C_A + C_{eq} + C_s)$	Contingency costs ($)	(38)
$CC = C_A + C_{eq} + C_s + C_{tr} + C_b + C_{en} + C_c$	Capital costs ($)	(39)
$Z = \frac{i(i+1)^m}{(i+1)^m}$	Amortization factor	(40)
$ACC = CC \cdot Z$	Capital annual costs ($/yr)	(41)
Operating cost		
$C_{th} = Q \cdot f \cdot 0.03 \cdot 365$	Thermal energy costs ($/yr)	(42)
$C_e = C_{el} \cdot P \cdot f \cdot Q \cdot 365$	Electricity ($/yr)	(43)
$C_l = 0.1 \cdot f \cdot Q \cdot 365$	Labor cost ($/yr)	(44)
$C_{ch} = 0.04 \cdot f \cdot Q \cdot 365$	Chemical material costs ($/yr)	(45)
$C_{in} = 0.005 \cdot C_A$	Insurance costs ($/yr)	(46)
$C_I = \alpha \cdot I_{total} \cdot C_{el} \cdot 24 \cdot f \cdot 365$	Exergy destruction cost ($/yr)	(47)
$AOC = C_{th} + C_e + C_l + C_{ch} + C_{in} + C_I$	Annual operating costs	(48)

The goodness of fit of the RSM models was tested using the multiple correlation coefficient (R^2). If the R^2 is closer to unity and in agreement with the value of the adjusted multiple correlation coefficient (adj. R^2), then the fit of the RSM model is valid.

In this study, RSM models were developed to investigate the effects of the three input variables on three responses. The input variables are S, ΔT, and Tph, and responses are TAC, GOR, and Q. The set of input conditions was obtained by using the design of experiments methodology. The central composite experimental design (CCD), with five level coded input factors ($-1.681, -1, 0, 1, +1.681$), was used. The designed set of data obtained by CCD, both in terms of the coded and actual values of the input variables, is presented in Tables 8 and 9. The theoretical model equations presented in Tables 1 to 7 were simulated for the values of the inputs as per CCD, and the corresponding output variables (TAC, GOR, Q) were calculated. The values of the theoretical model outputs are presented in Tables 8 and 9. These inputs–outputs data were subjected to multiple regressions by RSM using MINITAB 14 software.

2.4. Partial least squares (PLS)

Generally, the data from a chemical and environmental process are high dimensional and correlated. This high dimensionality and correlation is known to be an obstacle for the interpretation of the experiments and extraction of the process knowledge from data [27]. PLS is a multivariate iterative projection method, which models a relationship between independent variables (X) and dependent variables (Y). It models both sets of variables simultaneously, (X) and (Y), to find the latent variables (LVs) in X that will predict the latent variables in Y. In PLS modeling, data is divided into two groups of variables, X (descriptor) variables and Y (response) variables; a causal relationship is assumed to exist between them.

The PLS models are driven by a small number of latent variables (LVs) that are estimated as weighted averages of the independent variables. LVs are not directly measurable, but estimated from the data. Hence, they are often referred to as indirectly observed. The objective of PLS modeling is to model X in such a way that information in Y can be adequately predicted. The use of partial least squares to maximize the covariance between matrices X and Y builds a linear model by decomposing matrices X and Y into bilinear terms, which are given by Eqs. (59) and (60):

$$X = MG^T + E \tag{59}$$

$$Y = NH^T + K \tag{60}$$

where X and Y are independent and dependent matrices, M and N are latent score vectors, and G and H are corresponding loading vectors, which are applied to confirm the correlation between the independent and dependent variables. E and K are the matrices of the residuals. Loading weights represent the correlation between the independent and dependent variables; G and H are thus used to confirm the correlation of these variables [26,27].

In this study, the PLS method was used for multivariate analysis of the process. The LVs and loading vectors between independent variables and responses were obtained by using a code developed in MATLAB

2.5. Artificial neural network (ANN) modeling

In order to estimate and predict engineering properties that are functions of many variables and parameters, artificial neural network (ANN) is utilized as a computational tool. It transforms a non-linear, complex mathematical model into a simplified black-box structure. The ability of artificial neural network to represent nonlinear systems makes them a powerful tool for process modeling and much work has been reported over the last decade. The term ANN originates from research, which attempted to understand, and proposed simple models of, the operation of the human brain. Consequently, ANNs possess characteristics, in common with the biological system—they consist of numerous simple processing elements (neurons) joined together by variable strength connections (synapses) to form a massively

Table 7
Exergy destruction equations.

Equations	Descriptions	
$I_{sje} = S \cdot [(h_s - h_{v_{hc}}) - T_0(s_s - s_{v_{hc}})] - D_r \cdot [(h_{v_{hc}} - h_{v_n}) - T_0(s_{v_{hc}} - s_{v_n})]$	Exergy destruction of steam jet ejector	(49)
$I_{e_n} = [D_{n-1} + (D_1 + \ldots + D_{n-2} + D_r)(y-(n-1)F_n)y] \cdot L_{n-1}\left(1 - \frac{T_0}{T_{v1}}\right) + B_{n-1} \cdot SHC \cdot \left[\Delta T - T_0 Ln\left(\frac{T_{n-1}}{T_n}\right)\right] - D_n L_n\left(1 - \frac{T_0}{T_n}\right) - F_n \cdot SHC \cdot \left[(T_n - T_{fn}) - T_0 \cdot \ln\left(\frac{T_n}{T_{fn}}\right)\right]$	Exergy destruction of effects	(50)
$I_{con.} = [D_F + (D_r + D_1 + \ldots + D_{n-1}) \cdot y] \cdot Ln\left(1 - \frac{T_0}{T_n}\right) - m_{sw} \cdot SHC \cdot \left[(T_f - T_c) - T_0 \cdot Ln\left(\frac{T_f}{T_c}\right)\right]$	Exergy destruction of end condenser	(51)
$I_{D_r} = D_r \cdot SHC \cdot \left[(T_{v_n} - T_c) - T_0 \cdot \left(\frac{T_{v_n}}{T_c}\right)\right]$	Exergy destruction of freshwater recycled	(52)
$I_{D_{con.}} = D_{con.} \cdot SHC \cdot \left[(T_{v_n} - T_c) - T_0 \cdot \left(\frac{T_{v_n}}{T_c}\right)\right]$	Exergy destruction of end condenser distillate	(53)
$I_{B_n} = B_n \cdot SHC \cdot \left[(T_n - T_c) - T_0 \cdot \left(\frac{T_n}{T_c}\right)\right]$	Exergy destruction of Rejected brine	(54)
$I_{total} = I_{sje} + I_{e_n} + I_{con.} + I_{D_r} + I_{D_{con.}} + I_{B_n}$	Total exergy destruction	(55)

Table 8
Central composite design and mathematical responses for MED-TVC systems with 3 and 4 effects.

Set no.	Input variables						Responses for MED-TVC system with 3 effects			Responses for MED-TVC system with 4 effects		
	x_1	ΔT (K)	x_2	S (kg/s)	x_3	T_{ph} (K)	TAC ($/yr)	GOR	Q (m^3/d)	TAC ($/yr)	GOR	Q (m^3/d)
1	0	3.5	0	40	0	301.5	12,590,369	4.374	15,116	17,247,150	5.704	19,713
2	1	4.25	+1	50	+1	303.25	14,318,508	4.451	19,230	19,593,707	5.848	25,263
3	1.681	5	0	40	0	301.5	10,652,137	4.433	15,321	14,496,213	5.837	20,173
4	−1	2.75	+1	50	−1	299.75	18,351,253	4.3	18,576	25,263,623	5.57	24,063
5	0	3.5	0	40	0	301.5	12,590,369	4.374	15,116	17,247,150	5.704	19,713
6	1	4.25	−1	30	−1	299.75	8,500,520	4.356	11,290	11,556,144	5.692	14,754
7	0	3.5	1.681	60	0	301.5	18,887,219	4.374	22,676	25,873,787	5.705	29,573
8	0	3.5	0	40	−1.681	298	12,459,512	4.282	14,799	16,970,888	5.557	19,207
9	+1	4.25	+1	50	−1	299.75	14,169,290	4.356	18,819	19,262,590	5.693	24,593
10	0	3.5	−1.681	20	0	301.5	6,295,204	4.372	7555	8,624,672	5.703	9854
11	−1	2.75	+1	50	1	303.25	18,553,738	4.392	18,973	25,688,463	5.716	24,695
12	−1	2.75	−1	30	1	303.25	11,133,417	4.392	11,385	15,416,198	5.718	14,820
13	−1	2.75	−1	30	−1	299.75	11,009,171	4.299	11,144	15,155,234	5.569	14,435
14	+1	4.25	−1	30	1	303	8,583,891	4.444	11,518	11,741,644	5.836	15,126
15	−1.681	2	0	40	0	301.5	19,733,536	4.317	14,921	27,579,801	5.583	19,293
16	0	3.5	0	40	0	301.5	12,590,369	4.374	15,116	17,247,150	5.704	19,713
17	0	3.5	0	40	0	301.5	12,590,369	4.374	15,116	17,247,150	5.704	19,713
18	0	3.5	0	40	1.681	305	12,725,407	4.469	15,445	17,546,512	5.859	20,248
19	0	3.5	0	40	0	301.5	12,590,369	4.374	15,116	17,247,150	5.704	19,713
20	0	3.5	0	40	0	301.5	12,590,369	4.374	15,116	17,247,150	5.704	19,713

parallel and highly interconnected, information processing system. This gives the ANN several characteristics that are appealing for the modeling of nonlinear systems.

The majority of ANN architectures are multi-layer feed-forward networks that have one input layer, one or more hidden layers, and an output layer [28,29].

The general structure of a multi-layer feed-forward ANN with one hidden layer, which is used in this study, is shown in Fig. 9. The input layer consists of input variables, while the hidden and output layers consist of numerous individual units called neurons. Each neuron of these layers is a single computational processor that is connected to the input and output layers by weights and biases [30,29,20]. The output of neurons is given by Eq. (61) [13].

$$h_j = f\left(\sum W_{ji} X_i + b_j\right) \tag{61}$$

where i and j indicate the neurons in consecutive layers, h_j is the output of jth layer neuron, f is a suitable transfer function, X_i is the output of the ith layer neuron or the input to jth layer neuron, W_{ij} is the weight from the ith layer neuron to the jth layer neuron, and b_j is bias value of jth layer neuron.

The network is operated in two distinct phases called training and recall. When the network is trained, it can be used in the recall mode where the network weights are fixed and it tested with blind data sets. This testing or validation of a network is a very important step in the development cycle of a nonlinear neural network model. The overall goal is to develop a network, which can emulate the underlying system, which produced the training data [28].

The back-propagation (BP) algorithm is mostly used to train the multi-layer feed-forward ANN [29]. The goal of network training is to minimize the mean square error (MSE) between the measured value and the neural network output by adjusting its weights and biases.

In this study, separate ANN models were developed for MED-TVC systems using the neural network toolbox V4.0 of MATLAB 7.11. ΔT, S, and T_{ph} were considered as inputs, and TAC, GOR, and Q were considered as outputs for the ANN models. The datasets with factors (as per

Table 9
Central composite design and mathematical responses for MED-TVC systems with 5 and 6 effects.

Set no.	Input variables						Responses for MED-TVC system with 5 effects			Responses for MED-TVC system with 6 effects		
	x_1	ΔT (K)	x_2	S (kg/s)	x_3	T_{ph} (K)	TAC ($/yr)	GOR	Q (m^3/d)	TAC ($/yr)	GOR	Q (m^3/d)
1	0	3.5	0	40	0	301.5	19,341,482	7.017	24,250	22,653,766	8.362	28,898
2	1	4.25	+1	50	+1	303.25	22,032,100	7.262	31,373	25,992,793	8.759	37,839
3	1.681	5	0	40	0	301.5	16,261,413	7.281	25,162	19,289,724	8.842	30,557
4	−1	2.75	+1	50	−1	299.75	28,404,087	6.793	29,346	33,248,236	8.009	34,601
5	0	3.5	0	40	0	301.5	19,341,482	7.017	24,250	22,653,766	8.362	28,898
6	1	4.25	−1	30	−1	299.75	12,887,739	7.03	18,222	15,075,295	8.434	21,861
7	0	3.5	1.681	60	0	301.5	29,013,819	7.017	36,377	33,983,001	8.362	43,350
8	0	3.5	0	40	−1.681	298	18,907,181	6.802	23,509	21,998,099	8.065	27,872
9	+1	4.25	+1	50	−1	299.75	21,482,394	7.031	30,374	25,114,459	8.43	36,419
10	0	3.5	−1.681	20	0	301.5	9,668,348	7.015	12,122	11,330,131	8.36	14,447
11	−1	2.75	+1	50	1	303.25	29,047,655	7.005	30,261	34,199,388	8.299	35,852
12	−1	2.75	−1	30	1	303.25	17,434,736	7.007	18,163	20,524,703	8.298	21,509
13	−1	2.75	−1	30	−1	299.75	17,040,904	6.792	17,606	19,946,443	8.009	20,758
14	+1	4.25	−1	30	1	303	13,192,653	7.244	18,777	15,550,751	8.734	22,638
15	−1.681	2	0	40	0	301.5	31,409,363	6.785	23,448	37,143,671	7.958	27,503
16	0	3.5	0	40	0	301.5	19,341,482	7.017	24,250	22,653,766	8.362	28,898
17	0	3.5	0	40	0	301.5	19,341,482	7.017	24,250	22,653,766	8.362	28,898
18	0	3.5	0	40	1.681	305	19,812,214	7.245	25,039	23,380,779	8.682	30,004
19	0	3.5	0	40	0	301.5	19,341,482	7.017	24,250	22,653,766	8.362	28,898
20	0	3.5	0	40	0	301.5	19,341,482	7.017	24,250	22,653,766	8.362	28,898

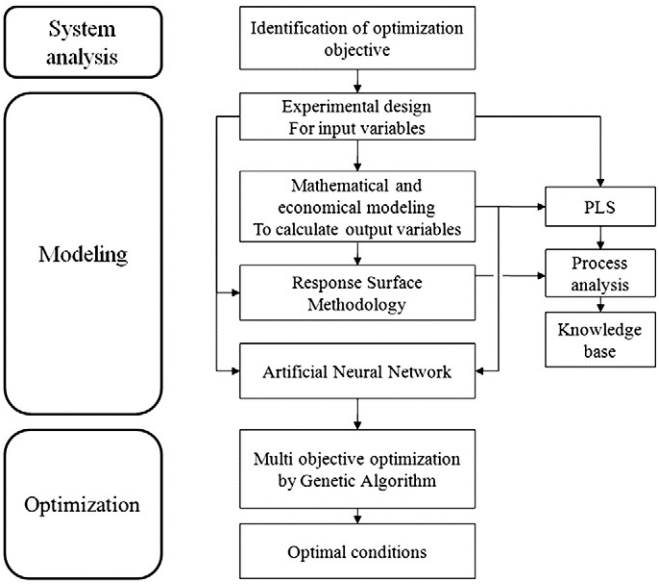

Fig. 2. Framework of the MED-TVC system optimization.

CCD design) and responses (obtained by theoretical model simulation) presented in Tables 8 and 9 were used for the training and validation of the ANN models. From total data set points, 70%, 15%, and 15% were randomly used for the training, validation, and testing of the ANN models, respectively. The hyperbolic tangent transfer function ('tansig' of MATLAB) was chosen for the neurons of the hidden layer, and a purely linear transfer function ('purelin' of MATLAB) was chosen for the output layer neuron. The mathematical definition of 'tansig' is given by Eq. (62) [31].

$$tansig = \frac{2}{1 + \exp\left(-2h_j\right)} - 1 \tag{62}$$

The optimum numbers of hidden layer neurons are determined based on the minimum value of the mean square error (MSE) obtained during training, and the values of the correlation coefficients for training and validation are achieved by examining different structures [33]. The numbers of hidden layer neurons obtained for ANN structures for MED-TVC systems with different numbers of evaporation effects are shown in Appendix A-3. The accuracy of the trained ANN model is tested using the correlation coefficient (R^2). As the R^2 approaches unity, the model achieves better performance. The developed ANN model was validated by using the testing data sets.

2.6. Multi objective optimization (MOO)

Almost all systems in chemical and mechanical engineering were optimized using a single objective function. Often the objective function accounted for the economic efficiency only, which is scalar quantity. In contrast, multi-objective optimization involves the simultaneous optimization of more than one objective function. Several industrial systems have been optimized over the last two decades with multiple objective functions and constraints, using a variety of algorithms. In such cases, one may get a set of several equally good (non-dominating) solutions, or, often, a Pareto front. The evolutionary genetic algorithm (GA) has become quite popular in recent years for solving problems involving a single and multiple objective functions [38]. A genetic algorithm (GA) is a class of parallel, iterative, and population-based search to find the optimal solution in a large solution domain by carrying out stochastic transformations inspired by natural evolution [32,30,19]. The basic building blocks of a genetic algorithm are genes that form chromosomes. Each gene controls one or more features of its chromosome. A collection of chromosomes creates a population. With a randomly generated population, the algorithm begins using three genetic operators: selection, crossover, and mutation [34–36]. On the basis of value of the individuals, the chromosomes are selected for transition from the current population by means of a selection process that is called the selection operator. Based on biological recombination, the crossover operator combines two chromosomes, called parents, to generate two similar children.

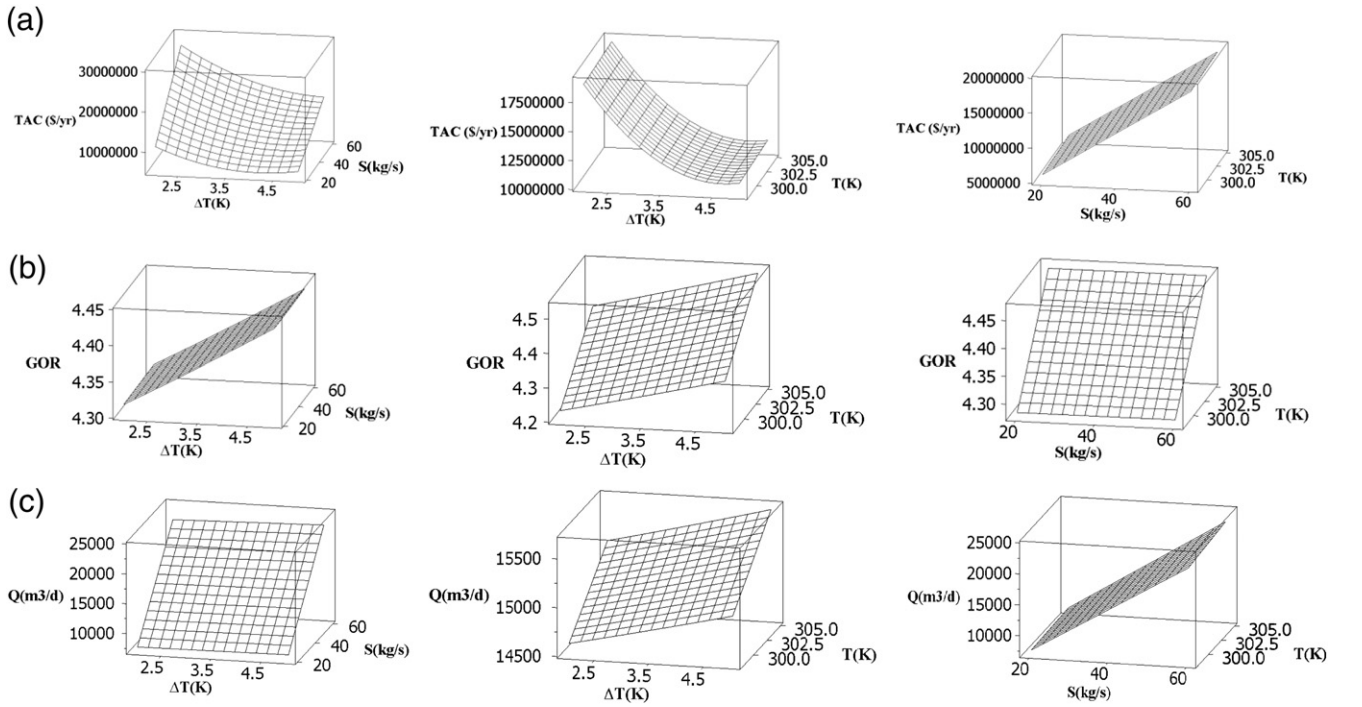

Fig. 3. Response surface plots for the effects of input variables on the responses for n = 3 (RSM model I); (a): Effect of the input variables on TAC. (b): Effect of the input variables on GOR. (c): Effect of the input variables on Q, (hold values are ΔT = 3.5 K, S = 40 kg/s, T = 301.5 K).

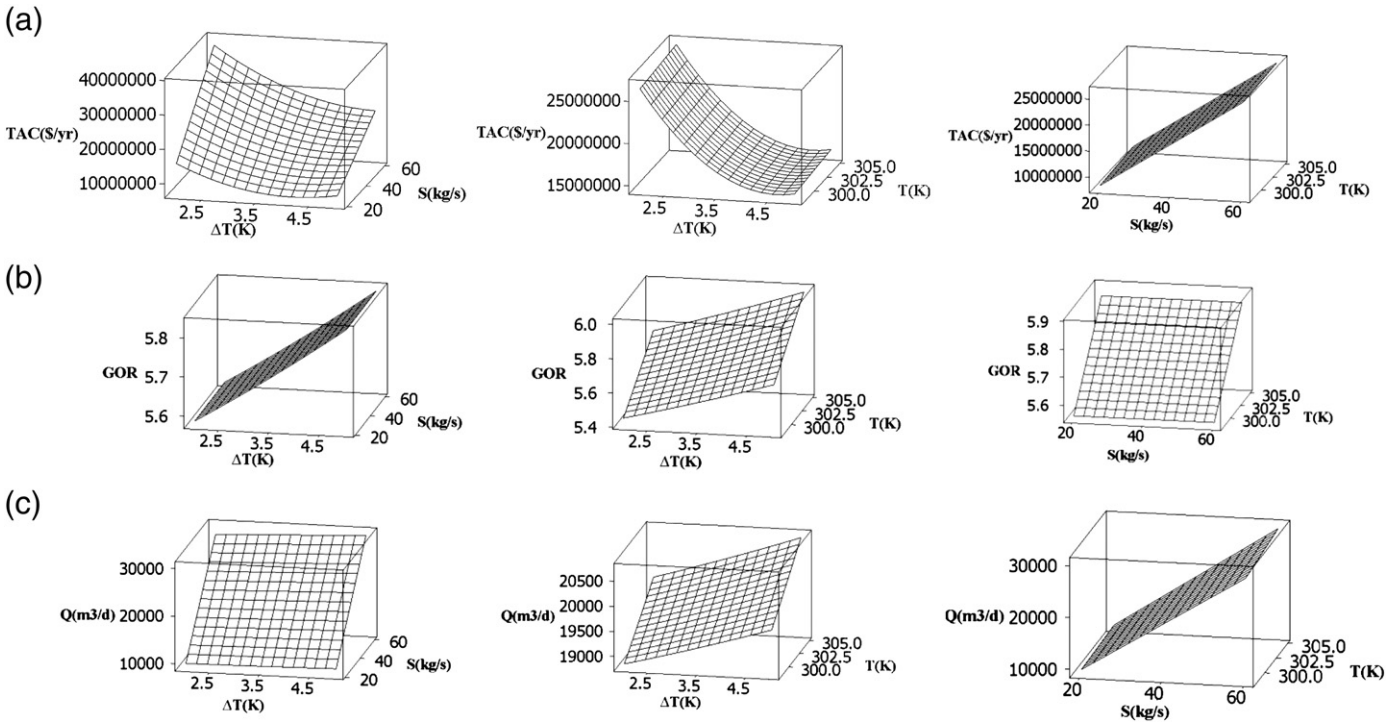

Fig. 4. Response surface plots for the effects of input variables on responses for n = 4 (RSM model II); (a): Effect of the input variables on TAC. (b): Effect of the input variables on GOR. (c): Effect of the input variables on Q. (hold values are ΔT = 3.5 K, S = 40 kg/s, T = 301.5 K).

The crossover operator continues until it completes the generation [30,34,36]. As the selection and crossover may become overzealous, the mutation operator performs random changes in the genes of existing chromosomes [36,37]. The total processes (selection, crossover, and mutation) are referred to as one generation. The generational cycle will stop when a desired termination criterion has been achieved [34]. In case of multi-objective problems, no single optimized solution could be achieved, and a search is generally performed

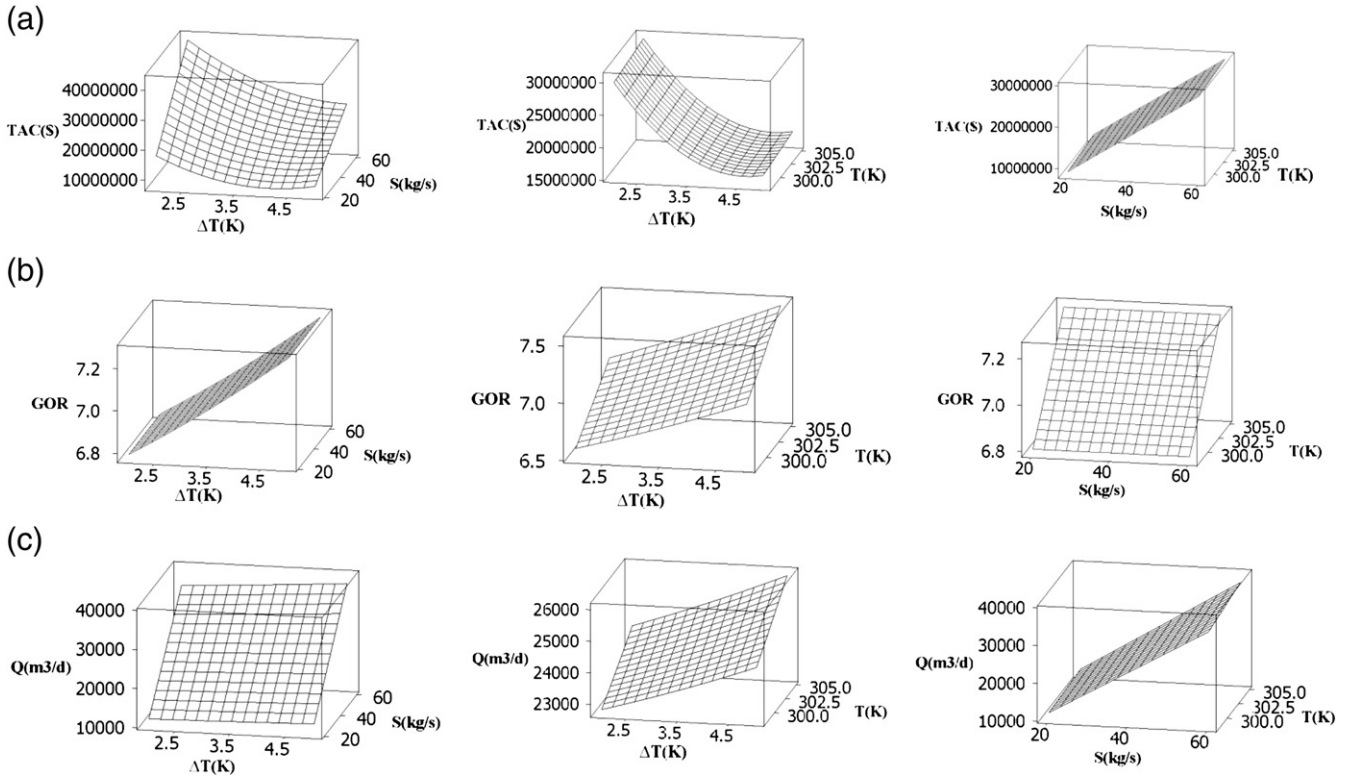

Fig. 5. Response surface plots for the effects of input variables on responses for n = 5 (RSM model III); (a): Effect of the input variables on TAC. (b): Effect of the input variables on GOR. (c): Effect of the input variables on Q. (hold values are ΔT = 3.5 K, S = 40 kg/s, T = 301.5 K).

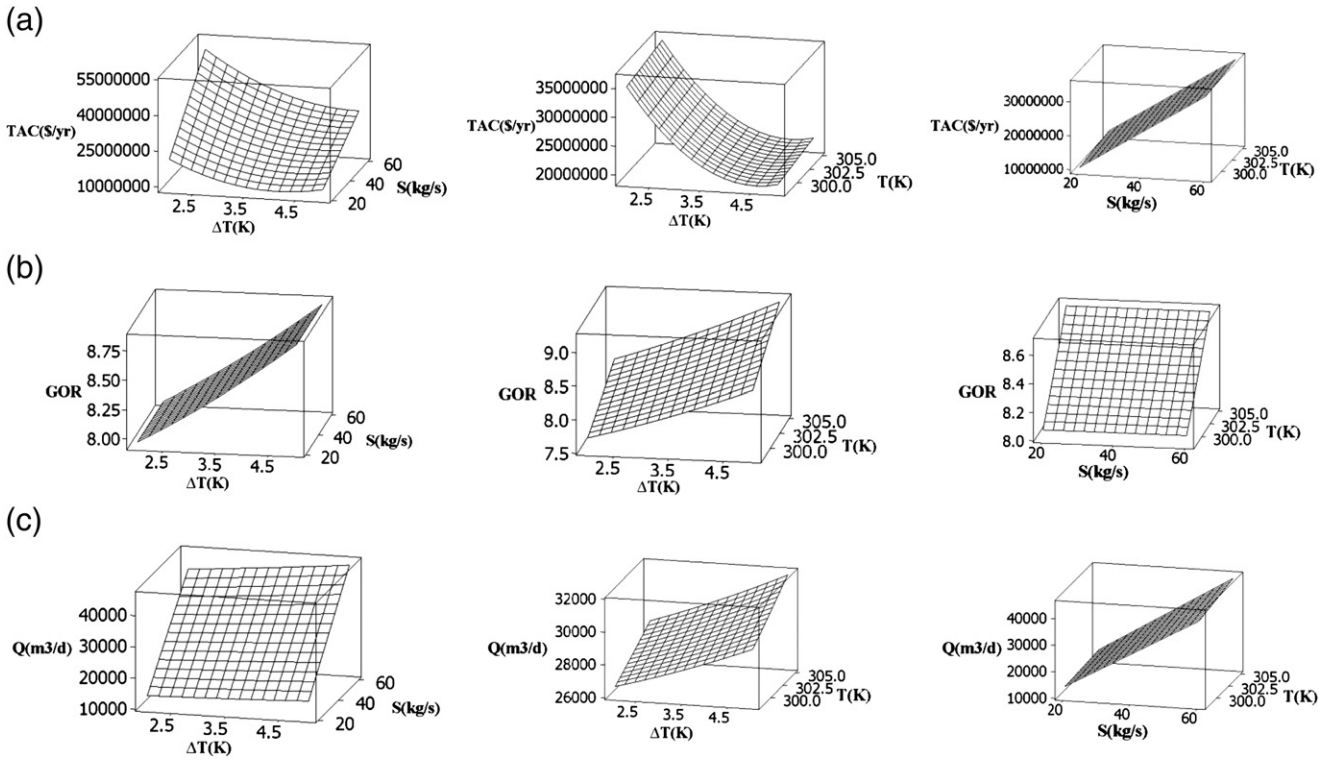

Fig. 6. Response surface plots for the effects of input variables on the responses for n = 6 (RSM model IV); (a): Effect of the input variables on TAC. (b): Effect of the input variables on GOR. (c): Effect of the input variables on Q. (hold values are ΔT = 3.5 K, S = 40 kg/s, T = 301.5 K).

following the concept of Pareto-optimality, where a set of solutions are developed providing the best possible compromises between the objectives. When several conflicting objective functions exist, the concept of "optimum" changes from the unique global optimum, as used in the single objective problems, to a set of solutions providing the best possible compromises between the objectives, known as the

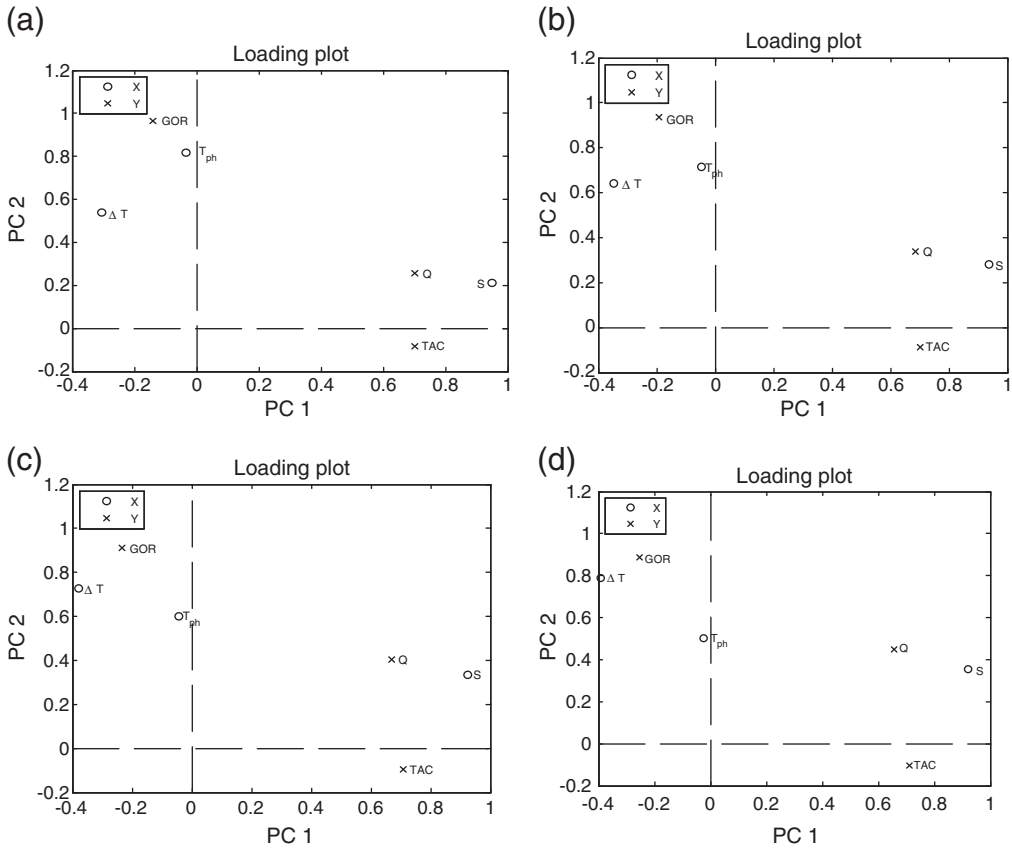

Fig. 7. Loading plots of the PLS model, (a) for n = 3, (b) for n = 4, (c) for n = 5, (d) for n = 6.

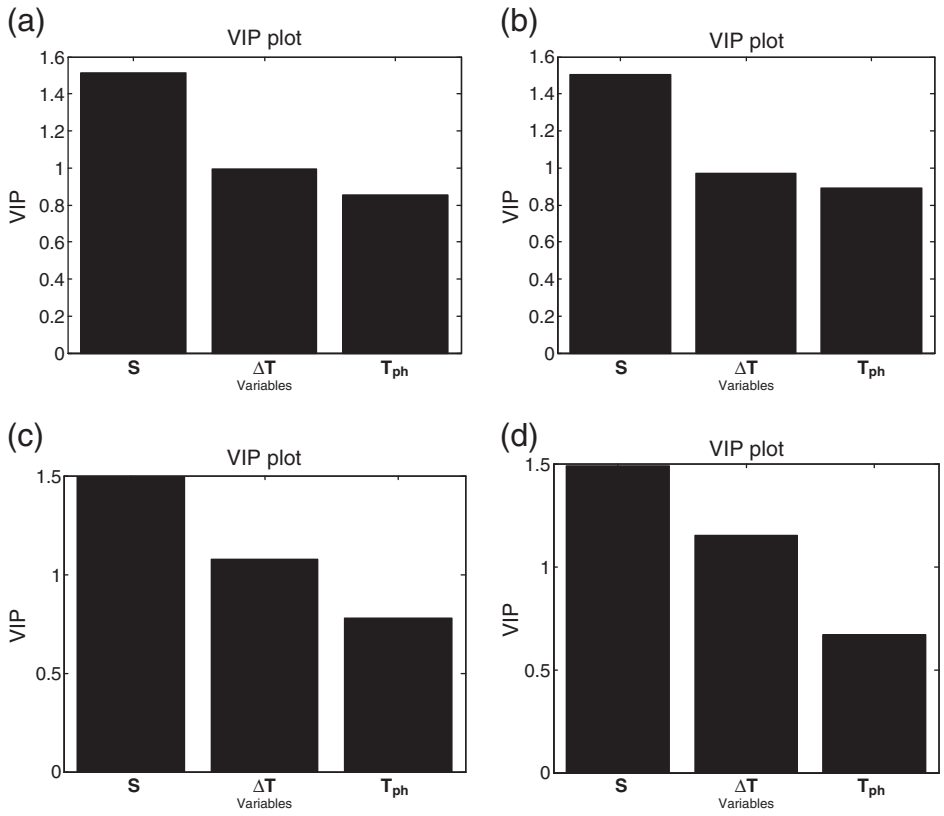

Fig. 8. VIP plots of the PLS model, (a) for n = 3, (b) for n = 4, (c) for n = 5, (d) for n = 6.

Pareto front. By the definition the Pareto-optimality, no other solution could exist in the feasible range that is at least as good as some member of the Pareto set, in terms of all the objectives, and strictly betters in terms of at least one [13]. Pareto set can provide useful insights to the decision-maker, who can then use his judgment or intuition to decide upon the preferred solution (operating point) [38].

In the present study, ANN models were used as the fitness functions for MOO, using GA with the 'gamultiobj' function in MATLAB 7.11, and the Pareto optimal solution sets were obtained for the MED-TVC systems with different numbers of effects. The MOO was used for the minimization of TAC and the maximization of GOR and Q, simultaneously. The independent variables of these functions are ΔT, S, and T_{ph}. The bounds of these variables are presented in Tables 8 and 9. Since the "gamultiobj" function minimizes the objective function, the GOR and Q functions were negated in order to convert into a minimization function.

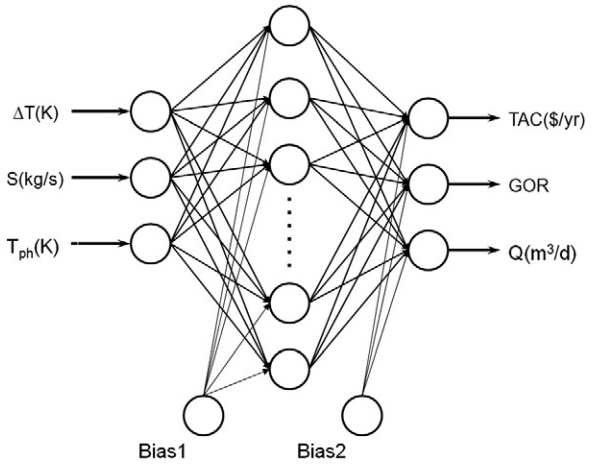

Fig. 9. General ANN structure for the prediction of TAC, GOR, and Q.

To better understand the optimal solutions and to obtain the best solution among the Pareto optimal solutions, TAC and Q were normalized by Eq. (63).

$$UPC = \frac{TAC}{Q \cdot 365 \cdot f} \tag{63}$$

where *UPC* is the unit product cost. Since the minimization of TAC and the maximization of Q were the objectives, the minimization of UPC was further investigated, instead of TAC and Q, in terms of choosing the best solution among the Pareto optimal solution set.

In order to obtain the Pareto optimal solution set for each system (with different n's), the population type was adjusted to 'double vector' with a size of 45. 'Tournament' with a size of 2 was selected as the selection function. 'Scattered' was chosen as the crossover function, with 0.8 as the crossover fraction. The creation and mutation functions were chosen to be 'uniform' and 'adaptive feasible', respectively. The direction, fraction, and interval of migration were set as 'forward', 0.2, and 20, respectively. The distance measure function and Pareto front population fraction were chosen to be 'distance crowding' and 0.35, respectively.

2.7. System optimization framework

The framework of the MED-TVC system optimization is shown in Fig. 2. First, the experimental design was defined, with ΔT, S, and T_{ph} as independent variables and TAC, GOR, and Q as response variables. The experimental design, using central composite design (CCD), determines the datasets used for the simulation of the theoretical model. Second, phenomenological and economic models were developed to calculate the corresponding output variables of the designed set data obtained by CCD, in terms of actual values. Exergy analysis was carried out to calculate the exergy destruction as lost opportunity cost. Third, PLS analysis was applied to evaluate the

correlation between the output variables (responses) and the input variables. Fourth, quadratic polynomial models were developed based on RSM in order to describe the relationship between the independent variables (inputs) and the dependent (responses) variables. Fifth, artificial neural network models were developed in order to apply them as objective functions of MOO. Sixth, multi-objective optimization was carried out to minimize TAC and maximize GOR and Q. The Pareto optimal front was obtained as a set of optimal solutions.

3. Results and discussions

3.1. Process analysis by RSM modeling

The values of three response variables corresponding to CCD data sets of three input variables were obtained for the MED-TVC systems with 3, 4, 5 and 6 effects by simulating the theoretical models. The actual and coded values of input variables of CCD data sets with the corresponding values of responses are presented in Tables 8 and 9. Each of input variables was consecutively coded as x_1, x_2 and x_3 at five levels: −1.681, −1, 0, 1 and 1.681.

According to Tables 8 and 9, the variation range of ΔT is from 2 K to 5 K, motive steam flow rate, S is in the range of 20 to 40 kg/s, and the range of Tph is from 298 K to 305 K. The central values chosen for the experimental design were ΔT = 3.5 k, S = 40 kg/s and T_{ph} = 301.5 k in uncoded form.

By applying multiple regression analysis on the design matrix and the responses presented in Tables 8 and 9, the RSM models I, II, III, and IV were developed for MED-TVC systems with 3, 4, 5, and 6 effects, respectively are presented in Table A-1 in Appendix-A. These RSM models can be used for the simulation of MED-TVC systems in order to obtain TAC, GOR, and Q.

The analysis of variance (ANOVA) is essential to test the significance of the model. Therefore, the ANOVA was conducted to test the significance of the fit of the second-order polynomial equation for the RSM models on the coded equations and the results are shown in Table A-2 in Appendix-A.

As seen in Table A-2, the ANOVA of the regression models showed that the quadratic model was highly significant, as was evident from the Fisher's *F*-test with a very low probability value P-value. As presented in Table A-2, for RSM model I, *F* value for TAC, GOR and Q are 429.16, 40191.6 and 40191.6, respectively and p-values are 0.000. Fisher's *F*-test calculated by MATLAB software are 2.96, 2.915 and 2.94. The calculated *F* values were found to be greater than the Fisher's *F*-test at the 5% level. As shown in Table A-2, similarly, for RSM models II, III, and V all of *F* values are greater than Fisher's *F*-test at the 5% level and P-values are 0.000. Since, in all of RSM models, calculated *F* values are greater than Fisher's *F*-test, the Fisher's *F*-test concluded with 95% certainly that the regression model explained a significant amount of the variation in the responses.

The goodness of fit of the model was checked by the multiple correlation coefficients (R^2). The values of R^2 for RSM models I, II, III and V are presented in Table A-2. For RSM model I, the values of R^2 for TAC, GOR and Q are 0.994, 1 and 1, respectively. These values indicate that the regression model of TAC did not explain only 0.6% of the total variations. Moreover, the regression models of GOR and Q explained all of total variations. In addition, the values of adjusted multiple correlation coefficient (adj. R^2) presented in Table A-2 are also very high, showing a high significant of the model.

Similarly, for RSM models II, III and V, R2 and adj. R2 are also very high, which indicate the goodness of fit of the models.

The response surface plots of TAC, GOR, and Q as functions of two factors were plotted using the RSM models presented in Table A-1 and these plots are shown in Figs. 3–6. Since the regression model has three factors, one factor was held constant at the center level (for the level in coded form: $x_i = 0$ or for the uncoded form $X_i = X_0$) for each plot.

3.1.1. Effect of input variables on the TAC, GOR, and Q

Figs. 3a–6a show the effects of input variables on the TAC for MED-TVC systems. The interaction effects occur only between ΔT and S, and there are not any interaction effects between ΔT and T_{ph} or S and T_{ph}. The effect of T_{ph} on the TAC appears to be negligible. The main effect of ΔT is higher than the main effect of S, and the effect of ΔT is quadratic, while the effect of S is almost linear. TAC decreases with increases in ΔT and with decrease in S.

Figs. 3b–6b illustrate the effects of varying the input variables on GOR. According to these figures, the GOR increases with increases in both ΔT and T_{ph}. The effect of ΔT is more significant at higher levels of T_{ph}, and the effect of T_{ph} is also more significant at higher levels of ΔT. The maximum value of GOR is achieved when ΔT and T_{ph} are at the maximum points in the range studied. The main effect of ΔT is found to be slightly larger than the main effect of T_{ph} and both of them have slight quadratic effects, while the effect of *S* on GOR is almost negligible.

The effects of input variables on Q are shown in Figs. 3c–6c. The main effect of S is higher than the main effect of ΔT. The maximum value of Q occurs at the maximum values of ΔT and T_{ph}. Studies on the interaction effects between ΔT and S as well as between T_{ph} and S revealed that the main effect of S is higher than that of ΔT and the main effect of S is higher than that of T_{ph}. Hence, the effects of T_{ph} on Q may be considered almost negligible in these interactions.

3.2. Process analysis by PLS methodology

PLS is a multivariate linear regression algorithm that is used for the multivariate analysis of MED-TVC desalination systems. Fig. 7 shows the loading plots in the PC1 and PC2. Herein, the Y variables are TAC, GOR, and Q, while X variables are ΔT, S, and T_{ph}. As shown in Fig. 7, the loading plots are divided into two clusters. One of the clusters consists of GOR, ΔT, and T_{ph}, and another includes TAC, Q, and S. The proximity of ΔT and T_{ph} on the plots and their proximity to GOR show that these two input variables are highly correlated and their effects on GOR are considerable. T_{ph} is shown to have a larger influence on GOR than ΔT does. The proximity of GOR, TAC, and S on the plots shows that the effects of S on GOR and TAC are considerable and that the effects of ΔT and T on GOR and TAC are negligible.

Fig. 8 shows the variable importance in the projection (VIP) plots by PLS loading weight. The VIP plots are introduced to account for the ways in which X variables contribute to Y variables. The variable that shows the highest value in the VIP plot is the most important variable in terms of its influence on the process performance. As shown in Fig. 8, in terms of MED-TVC systems, S is the most important variable and has the most influence on the process. The influence of ΔT appears to be higher than that of T_{ph}.

3.3. ANN modeling

The structures of the ANN models were obtained by training and error methods based on MSE and R^2 values. The optimal numbers of hidden layer neurons were defined based on the minimum values of MSE and R^2 for training and validation, which were determined by training the different feed-forward networks of various structures. The obtained numbers of hidden layer neurons based on acceptable MSE values (MSE ≤ 0.005) along with the weights and biases are presented in Table A-3 in Appendix A.

The predicted values, using ANN, versus the actual values, using the theoretical model, for MED-TVC systems with different *n* values are shown in Figs. 10 and 11, respectively. The best fit lines with the best linear equations and correlation coefficients (R^2) for the training data sets and the validation data sets are presented in Figs. 10 and 11, respectively. As shown in Fig. 10a–10d and Table A-3, the MSE of trained networks are 0.00052, 0.000046, 0.0025, and 0.00153 for systems with 3, 4, 5 and 6 effects, respectively and the correlation

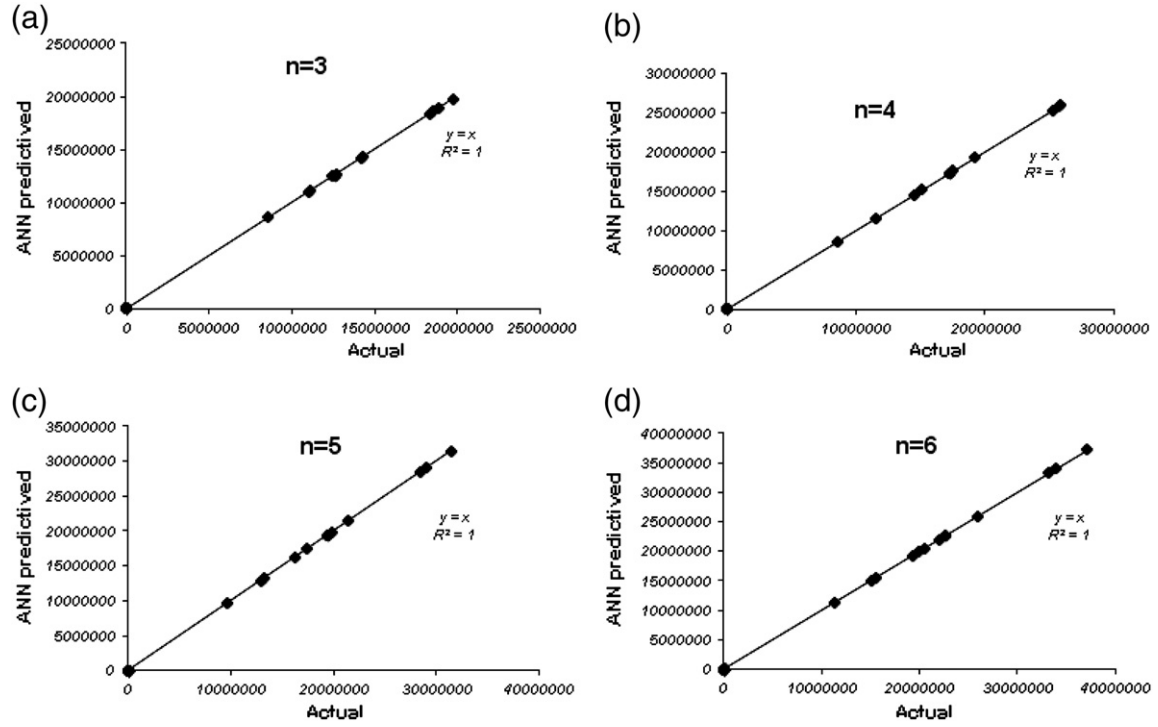

Fig. 10. Regression plots for the ANN training data sets, (a) n = 3, (b) n = 4, (c) n = 5, (d) n = 6.

coefficients' (R^2) values are equal to unity, which means the points of the training data sets perfectly fit the model.

As shown in Fig. 11a–11d, the validation and testing data points aren't completely on the y = x line and are distributed around x = y line in a narrow area. The best fit line equations of the validation and testing data are y = 1.058x, y = 0.981x, y = 1.041x, and y = 1.018x, and their correlation coefficients are 0.982, 0.993, 0.994, and 0.997, respectively.

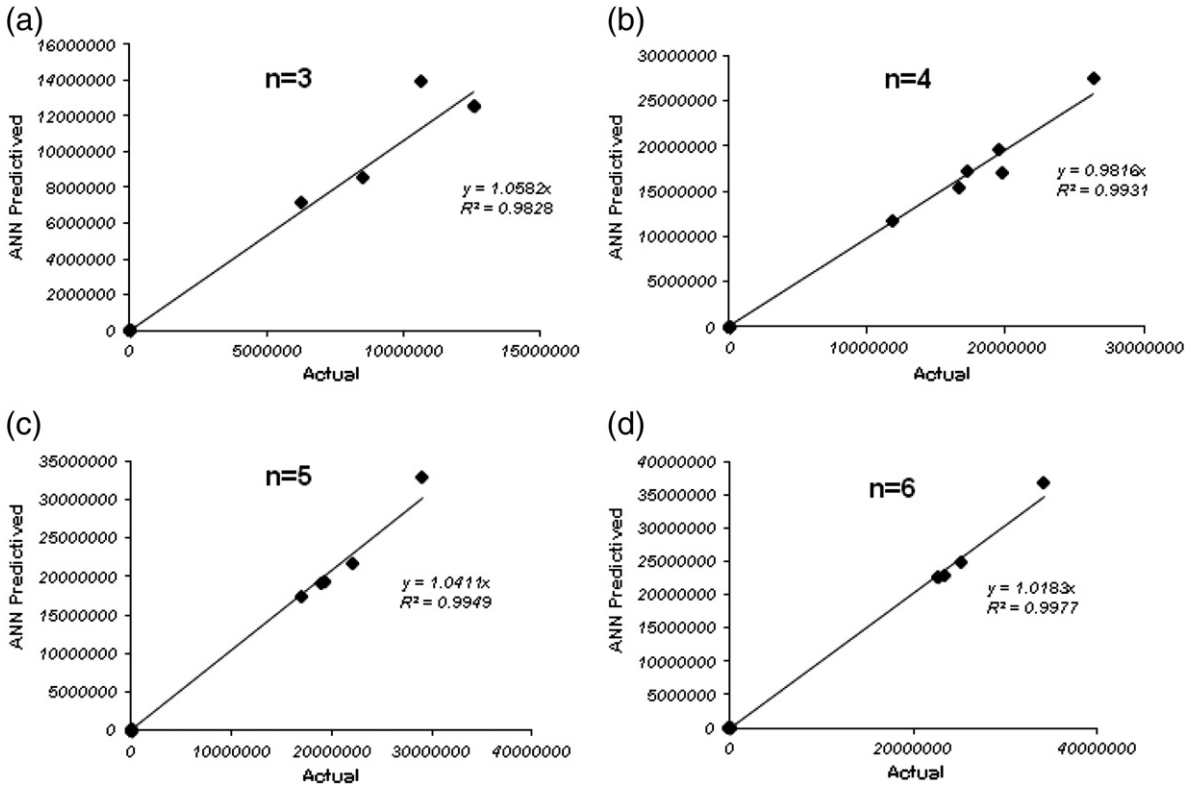

Fig. 11. Regression plots for the ANN validation data sets, (a) n = 3, (b) n = 4, (c) n = 5, (d) n = 6.

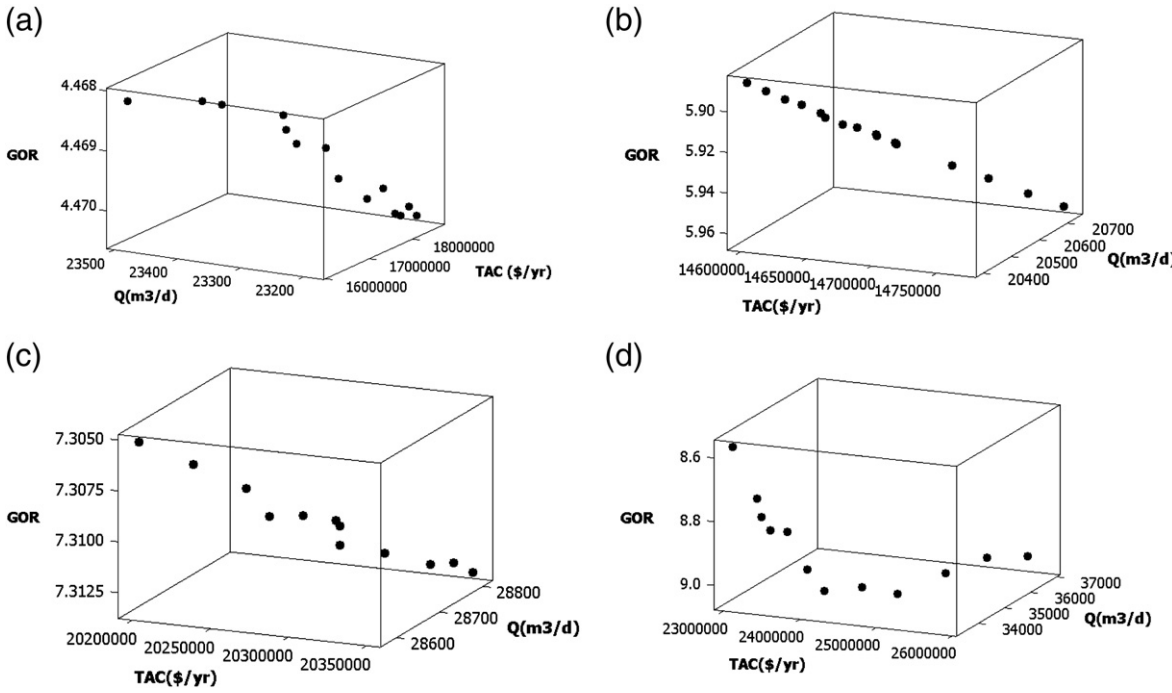

Fig. 12. Pareto optimal solution for TAC, GOR, and Q, using multi-objective optimization. a: Pareto optimal solutions for n = 3, b: Pareto optimal solutions for n = 4, c: Pareto optimal solutions for n = 5, d: Pareto optimal solutions for n = 6.

Since the correlation coefficient values of the training data sets are equal to unity and the correlation coefficient values of the testing and validation data sets are very close to unity as well as the MSE values are less than acceptable value (0.005), the ANN models presented in Table A-3 in Appendix-A can be considered to be valid models for representing the data. According to Table A-3, for systems with 3, 4, 5 and 6 effects, the optimal number of hidden layer is 1 with number of neurons 5, 7, 6 and 6 respectively.

3.4. Multi-objective optimization

The Pareto optimal solution obtained by using GA for MOO to minimize TAC and to maximize GOR and Q for MED-TVC systems with different values of *n* are presented in Fig. 12. The ANN models developed were used as the fitness functions for GA. Each point of the Pareto set (a set of TAC, GOR, and Q) is associated with a set of input decision variables (a set of ΔT, S and T_{ph}).

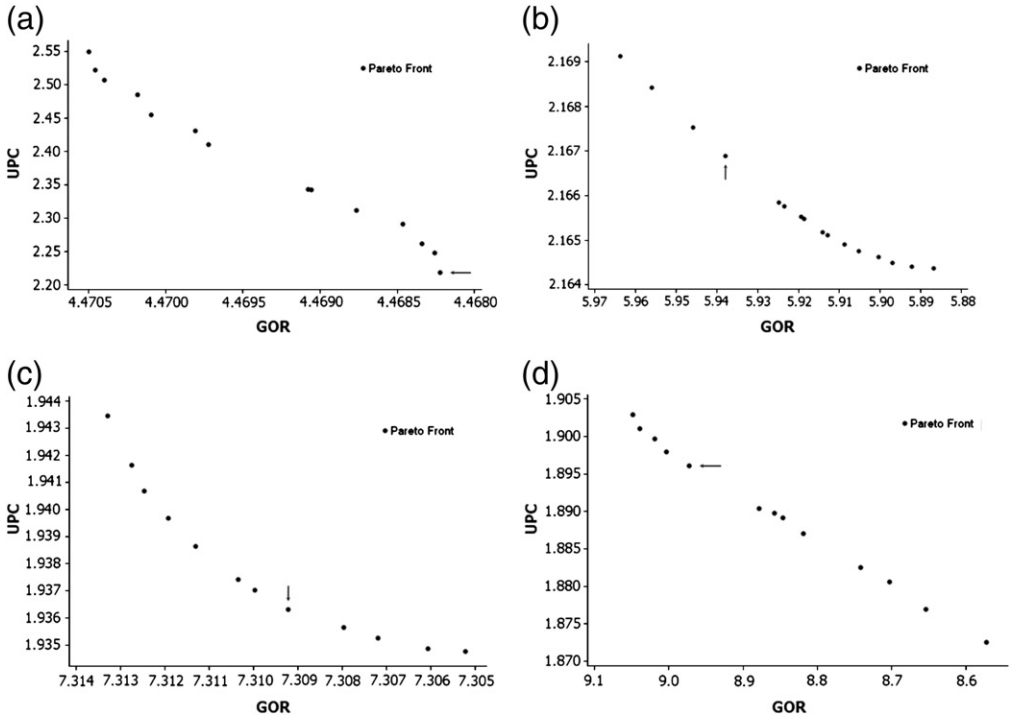

Fig. 13. Pareto optimal solutions for UPC and GOR. a: Pareto optimal solutions for n = 3, b: Pareto optimal solutions for n = 4, c: Pareto optimal solutions for n = 5, d: Pareto optimal solutions for n = 6.

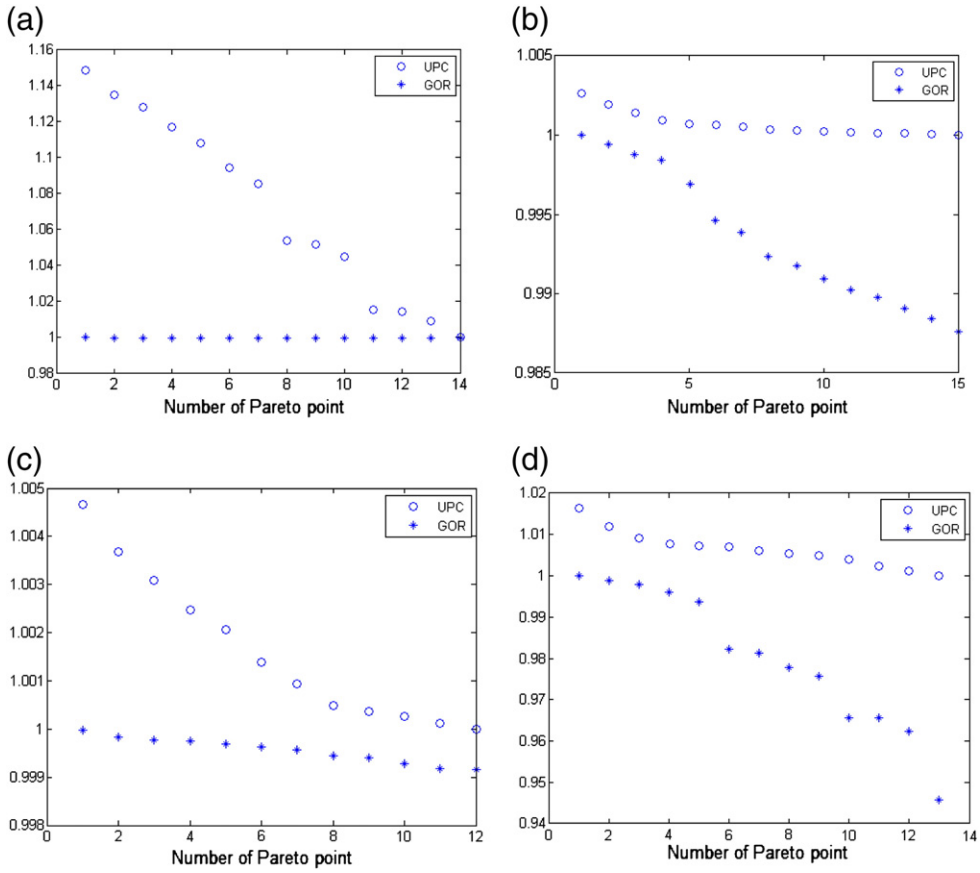

Fig. 14. Variations of normalized UPC and GOR VS Pareto optimal solution number. a: for n = 3, b: for n = 4, c: for n = 5, d: for n = 6.

In order to better investigate the Pareto front, 3-dimensional Pareto plots, which are shown in Fig. 12, were converted to 2-dimensional plots with UPC and GOR axes using Eq. (63). 2-dimentional Pareto plots are shown in Fig. 13.

In order to select the best point from among the Pareto solution points (Fig. 13), the values of UPC and GOR were normalized. Fig. 14 shows the variations of normalized GOR and UPC for each Pareto points for systems with different *n*.

Fig. 14a shows the variations of UPC and GOR for system with 3 effects. Since, variations of GOR are negligible and Pareto point 14 has minimum value of UPC among the Pareto points, therefore, Pareto point 14 can be selected as the best operation point for system with 3 effects. This point is indicated by an arrow in Fig. 13a. According to Figs. 12a and 13a, the UPC, GOR, Q and TAC of selected point are 2.2 $/m^3, 4.468, 23,264 m^3 and 16,889,664 $/yr, respectively.

As shown in Fig. 14b, the values of UPC are decreased from points 1 to 4 and are approximately constant from points 4 to 16. The values of GOR are decreased slightly till point 4 and then decreased sharply. Since, Pareto point 4 has minimum value of UPC and maximum value of GOR, simultaneously, among the Pareto solution points; therefore, Pareto point 4 can be selected as the best operation point for system with 4 effects. This point is presented by an arrow in Fig. 13b. When the system operates based on the selected point the values of UPC, GOR, Q, and TAC are 2.167 $/m^3, 5.938, 25,437 m^3 and 18,190,253 $/yr, respectively.

The variations of normalized UPC and GOR for system with 5 effects are shown in Fig. 14c. As shown in Fig. 14c, the values of UPC are decreased from points 1 to 8 and are approximately constant from points 8 to 12. Also, the values of GOR are decreased slightly. Since, variations of GOR are very slight and Pareto point 8 has approximately minimum value of UPC, therefore, Pareto point 8 can be selected as the best operation point for MED-TVC system with 5 effects. Selected point is presented by arrow in Fig. 13c. According to Figs. 12c and 13c, When the system operates based on the selected point the values of UPC, GOR, Q, and TAC are 1.936 $/m^3, 7.31, 28,577 m^3 and 18,958,264 $/yr, respectively.

Fig. 14d shows the variations of UPC and GOR for system with 6 effects. As shown in Fig. 14d, the values of UPC are decreased from points 1 to 5 and are approximately constant from points 5 to 15. The values of GOR are decreased slightly till point 5 and then decreased sharply to point 15. Since, Pareto point 5 has minimum value of UPC and maximum value of GOR, simultaneously, among the Pareto solution points; therefore, Pareto point 5 can be selected as the best operation point. This point is presented by arrow in Fig. 13d. When the system with 6 effects operates based on the selected point the values of UPC, GOR, Q, and TAC are 1.895 $/m^3, 8.97, 34,005 m^3 and 21,265,026 $/yr, respectively.

According to Table 10, with increase in the number of effects, the value of UPC is decreased and the value of GOR is increased. Among the MED-TVC systems, the minimum value of UPC is 1.895 $/m^3 and the maximum value of GOR is 8.97, which are relevant to the

Table 10
Input decision variables corresponding to each of the preferred points, as depicted in Fig. 13.

Effects no.	UPC ($/m^3)	GOR	Q (m^3/d)	TAC ($n)	ΔT (K)	S (kg/s)	T_{ph} (K)
n = 3	2.2	4.468	23,264	16,889,664	5	60	305
n = 4	2.167	5.938	25,437	18,190,253	5	55	303.2
n = 5	1.936	7.31	28,577	18,958,264	5	45	302.1
n = 6	1.895	8.97	34,005	21,265,026	5	44	300.5

MED-TVC system with 6 effects. Also, the maximum value of UPC is 2.2 $/m^3 and the minimum value of GOR is 4.468 which are relevant to the MED-TVC system with 3 effects.

Based on summarized results in Table 10, the system with 6 effects reduces UPC by 14%, 12.5%, 2% and increases GOR by 50%, 34% and 18% in theoretical aspect compared to systems with 3, 4 and 5 effects, respectively. It means that, the influence of the effect number increasing on the GOR is greater than UPC.

The sets of input decision variables corresponding to selected points as design parameters are tabulated in Table 10. As presented in Table 10 the values of ΔT, S and T_{ph} corresponding to best Pareto point for system with 6 effects are 5 k, 44 kg/s and 301 k, which are introduced as the optimal design parameters.

4. Conclusions

In this study, a new approach to the optimization of MED-TVC desalination systems has been presented. The following conclusions can be drawn:

1. Through analysis of the RSM and PLS models, ΔT and T_{ph} were found to have significant effects on GOR compared to that of S, while the effect of S on the TAC and Q were considerable compared to those of ΔT and T_{ph}.
2. Increasing the number of effects increased the values of TAC and Q, but the increase in these parameters decreased the value of UPC in the MED-TVC system. The system with six effects was shown to have the minimum value of UPC.
3. An increase in the number of effects caused an increase in the value of GOR, as indicated by the maximum value of GOR obtained with the MED-TVC system of six effects.
4. Best Pareto solution was selected from among the Pareto sets. Among the MED-TVC systems with 3, 4, 5 and 6 effects, the system with six effects was presented as the best system, with the minimum value of UPC and maximum value of GOR. The MED-TVC system with 6 effects reduces UPC by 14%, 12.5%, 2% and increases GOR by 50%, 34% and 18% in theoretical aspect compared to systems with 3, 4 and 5 effects, respectively.

Nomenclature

A	Heat transfer area, m^2
ACC	Annual capital cost, $/yr
ANN	Artificial neural network
AOC	Annual operating cost, $/yr
B	Brine blow down mass flow rate, kg/s
BP	Back-propagation
BPE	Boiling point evaluation, °C
B	Bias
C	Concentration, ppm
C_A	Area cost, $
C_b	Building cost, $
C_c	Contingency cost, $
C_{ch}	Chemical materials cost, $/yr
C_e	Electricity cost, $/yr
C_{el}	Unit product electricity cost, $/kWh
C_{en}	Engineer and salary cost, $
C_{eq}	Instrument cost, $
C_I	Exergy destruction cost, $/yr
C_{in}	Insurance cost, $/yr
C_l	Labor cost, $/yr
Cp	Specific heat capacity, kJ/kg°C
C_s	Site cost, $
C_{th}	Thermal energy cost, $/yr
CC	Capital cost, $
CCD	Central composite design
D	Distillate, kg/s
E	Matrix of residual
F	Mass flow rate of feed seawater, kg/s
f	Plant load factor
G	Corresponding loading vector
GA	Genetic algorithm
GOR	Gain output ratio (as optimized parameter)
H	Corresponding loading vector
h	Specific enthalpy, kJ/kg
i	Interest rate
I	Exergy destruction (kW)
K	Matrix of residual
L	Latent heat, kJ/kg
LV	Latent variable
LMTD	Logarithmic mean temperature difference
M	Latent score vector
MED-TVC	multi effects distillation-thermal Vapor compression
MOO	Multi objective optimization
MSE	Mean square error
m	Plant life cycle
N	Latent score vector
NEA	Non-equilibrium allowance
PCA	Principal component analysis
PE	Process element
Q	Fresh water flow rate (as optimized parameter)
R^2	Coefficient of multiple determination
S	Motive steam mass flow rate, kg/s (as variable)
s	Specific entropy, kJ/kg k
SHC	Specific heat, kJ/kg k
SJE	Steam jet ejector
T	Temperature, °C
$\bar{T}$	Temperature of brine after cooling
T′	Temperature of brine in each effect
T_{ph}	Pre-heated seawater temperature, $°C_{(as\ variable)}$
TAC	Total annual cost, $/yr (as optimized parameter)
TBT	Top brine temperature, °C
U	Heat transfer coefficient, kW/m^2 k
UPC	Unit product cost, $/$m^3$ (as optimized parameter)
W	Weight
X	Input variable
X	Dimensionless coded variable
Y	Output variable
Y	Flashing fraction
Z	Amortization factor

subscripts

C	Condensate
Con.	Condenser
E	Effect
H	Pre-heater
N	Number of effect
Ph	Preheated feed water
R	Entrained steam
S	Steam
Sw	Seawater
V	Vapor

Greek

A	Avoidable exergy destruction coefficient
B	Regression coefficient within response surface model
ΔT	Temperature different between effects (as variable)

Acknowledgements

This work was supported by the Korea Science and Engineering Foundation (KOSEF) grant funded by the Korea government (MEST)

(KRF-2009-0076129) and the National Research Foundation of Korea (NRF) grant funded by Korea government (MEST) (No. 2012-0000609).

Appendix A

Table A-1. RSM models based on uncoded factors

RSM model I (n = 3)

$TAC = 3345508 - 8365518\Delta T + 517383S + 38723T_{ph} + 1139373\Delta T^2 - 56145S\Delta T$

$GOR = 9.793 - 0.10449\Delta T + 3.1938\times10^{-5}S - 0.0619361T_{ph} + 0.000568\Delta T^2 + 0.000144T_{ph}^2 + 0.000461T_{ph}\Delta T$

$Q = 48429 - 571.768\Delta T - 324.524S - 315.390T_{ph} + 2.33841\Delta T^2 + 0.513652{T_{ph}}^2 + 3.38109S\Delta T + 1.83499T_{ph}\Delta T + 2.29095ST_{ph}$

RSM model II (n = 4)

$TAC = -3469216 - 12177777\Delta T + 722619S + 84015.5T_{ph} + 1659082\Delta T^2 - 80719.1S\Delta T$

$GOR = 23.9648 - 0.374243\Delta T + 2.9128\times10^{-5}S - 0.160968T_{ph} + 0.00268\Delta T^2 + 0.00033T_{ph}^2 + 0.001459T_{ph}\Delta T$

$Q = 114137 - 1657.53\Delta T - 640.899S - 739.883T_{ph} + 8.93063\Delta T^2 + 1.19961{T_{ph}}^2 + 7.38297S\Delta T + 5.28175T_{ph}\Delta T + 3.67530ST_{ph}$

RSM model III (n = 5)

$TAC = -14046877 - 14436144\Delta T + 819391S + 132529T_{ph} + 1967137\Delta T^2 - 92918.9S\Delta T$

$GOR = 41.3513 - 0.889767\Delta T + 3.17314\times10^{-5}S - 0.282743T_{ph} + 0.007237\Delta T^2 + 0.0005546{T_{ph}}^2 + 0.00333T_{ph}\Delta T$

$Q = 19587 - 3858.7\Delta T - 1071.66S - 1257.63T_{ph} + 24.6750\Delta T^2 + 2.01983{T_{ph}}^2 + 14.4136S\Delta T + 12.2046T_{ph}\Delta T + 5.39894ST_{ph}$

RSM model V (n = 6)

$TAC = -29155538 - 17825555\Delta T + 961301S + 202641T_{ph} + 2433707\Delta T^2 - 109099S\Delta T$

$GOR = 76.3191 - 1.95501\Delta T + 1.16886\times10^{-5}S - 0.519600T_{ph} + 0.0170351\Delta T^2 + 0.0009667{T_{ph}}^2 + 0.00706T_{ph}\Delta T$

$Q = 331523 - 7906.85\Delta T - 1683.46S - 2104.69T_{ph} + 58.8611\Delta T^2 + 3.34092{T_{ph}}^2 + 25.1448S\Delta T + 24.8971T_{ph}\Delta T + 7.68986ST_{ph}$

Table A-2. Results of ANOVA for RSM models

RSM model I (n = 3)

Source	Degree of freedom	Sum of squares	Mean square	F-value	P-value
TAC					
$R^2 = 0.994$, adj. $R^2 = 0.991$					
Fisher's *F*-test = 2.96					
Regression	5	2.40014E + 14	4.80027E + 13	429.16	0.000
Residual	14	1.56594E + 12	1.11853E + 11		
Total	19	2.41580E + 14			
GOR					
$R^2 = 1$, adj. $R^2 = 1$					
Fisher's *F*-test = 2.915					
Regression	6	0.047446	0.007908	40191.60	0.000
Residual	13	0.000003	0.000000		
Total	19	0.047449			
Q					
$R^2 = 1$, adj. $R^2 = 1$					
Fisher's *F*-test = 2.94					
Regression	8	0.047446	0.007908	40191.60	0.000
Residual	11	0.000003	0.000000		
Total	19	0.047449			

Table A-2 (*continued*)

RSM model I (n = 3)

Source	Degree of freedom	Sum of squares	Mean square	F-value	P-value

RSM model II (n = 4)

Source	Degree of freedom	Sum of squares	Mean square	F-value	P-value
TAC					
$R^2 = 0.993$, adj. $R^2 = 0.990$					
Fisher's *F*-test = 2.96					
Regression	5	4.66616E + 14	9.33232E + 13	395.34	0.000
Residual	14	3.30483E + 12	2.36059E + 11		
Total	19	4.69921E + 14			
GOR					
$R^2 = 1$, adj. $R^2 = 1$					
Fisher's *F*-test = 2.915					
Regression	6	0.152863	0.025477	80228.75	0.000
Residual	13	0.000004	0.000000		
Total	19	0.152867			
Q					
$R^2 = 1$, adj. $R^2 = 1$					
Fisher's *F*-test = 2.94					
Regression	8	391,139,716	48,892,465	7542511.30	0.000
Residual	11	71	6		
Total	19	391,139,788			

RSM model III (n = 5)

Source	Degree of freedom	Sum of squares	Mean square	F-value	P-value
TAC					
$R^2 = 0.992$, adj. $R^2 = 0.990$					
Fisher's *F*-test = 2.96					
Regression	5	6.02145E + 14	1.20429E + 14	370.02	0.000
Residual	14	4.55647E + 12	3.25462E + 11		
Total	19	6.06701E + 14			
GOR					
$R^2 = 1$, adj. $R^2 = 1$					
Fisher's *F*-test = 2.915					
Regression	6	0.434437	0.072406	122636.02	0.000
Residual	13	0.000008	0.000001		
Total	19	0.434445			
Q					
$R^2 = 1$, adj. $R^2 = 1$					
Fisher's *F*-test = 2.94					
Regression	8	594,621,538	74,327,692	2788825.99	0.000
Residual	11	293	27		
Total	19	594,621,831			

RSM model V (n = 6)

Source	Degree of freedom	Sum of squares	Mean square	F-value	P-value
TAC					
$R^2 = 0.992$, adj. $R^2 = 0.989$					
Fisher's *F*-test = 2.96					
Regression	5	8.35438E + 14	1.67088E + 14	353.84	0.000
Residual	14	6.61102E + 12	4.72216E + 11		
Total	19	8.42049E + 14			
GOR					
$R^2 = 1$, adj. $R^2 = 1$					
Fisher's *F*-test = 2.915					
Regression	6	1.14580	0.190967	192115.30	0.000
Residual	13	0.00001	0.000001		
Total	19	1.14582			
Q					
$R^2 = 1$, adj. $R^2 = 1$					
Fisher's *F*-test = 2.94					
Regression	8	851,597,568	106,449,696	1027627.90	0.000
Residual	11	1139	104		
Total	19	851,598,708			

Table A-3. Number of hidden layer neurons, network weights, and bias values with MSE for training of the ANN models

n = 3

Number of hidden layer neurons 5

MSE 0.00052

	Input layer to hidden layer weights				Hidden layer to output layer weights					
	W_1(input 1)	W_1(input 2)	W_1(input 3)	Bias	W_2 PE1	W_2 PE2	W_2 PE3	W_2 PE4	W_2 PE5	Bias
PE1*	2.0463	1.0168	−0.0097	−2.0368	0.4352	−0.4802	0.0964	−0.5377	0.8424	1.2154
PE2	0.5046	−2.3570	−0.0306	−0.9474	−0.4423	−0.2168	0.6743	−0.1011	0.43667	−0.2509
PE3	1.7209	−3.6087	0.0962	0.8429	1.2638	−0.5478	0.4208	−0.7847	−0.9962	0.2990
PE4	1.9190	−2.4935	−0.0931	1.4892						
PE5	−1.2940	−0.0769	−0.0082	−1.7514						

n = 4

Number of hidden layer neurons 7

MSE 0.000046

	Input layer to hidden layer weights				Hidden layer to output layer weights							
	W_1(input 1)	W_1(input 2)	W_1(input 3)	Bias	W_2 PE1	W_2 PE2	W_2 PE3	W_2 PE4	W_2 PE5	W_2 PE6	W_2 PE7	Bias
PE1	−1.6308	1.7725	0.7354	2.4158	0.8709	0.2667	0.3088	0.1310	−0.9929	0.2605	−0.1064	−0.2372
PE2	1.4107	1.5686	−1.6559	−1.7131	−0.9443	0.0650	−0.0776	−0.5278	−0.5464	0.6083	0.3882	0.2116
PE3	2.1359	1.3441	−0.5654	0.0391	0.8696	0.1954	0.3648	−0.1145	−0.5796	0.0279	−0.2608	−0.1421
PE4	−1.9928	−0.7886	−1.5761	−0.2314								
PE5	1.3099	−1.2354	−0.3538	0.6637								
PE6	0.4948	−2.4152	0.6294	1.6025								
PE7	1.6637	−0.6286	1.5534	3.2583								

Number of hidden layer neurons 6

	Input layer to hidden layer weights				Hidden layer to output layer weights						
	W_1(input 1)	W_1(input 2)	W_1(input 3)	Bias	W_2 PE1	W_2 PE2	W_2 PE3	W_2 PE4	W_2 PE5	W_2 PE6	Bias
n = 5											
MSE 0.0025											
PE1	−1.1598	1.9389	0.8749	2.6098	1.2019	−1.0506	0.9934	0.3470	0.0634	0.0165	−0.1093
PE2	−2.2990	1.3788	1.1684	2.4769	0.5032	−0.4662	−0.4353	0.1934	0.7164	0.0313	0.5065
PE3	−1.0793	1.8029	−0.3064	−0.1653	1.2553	0.0405	0.1959	−0.3196	0.4114	−0.3883	−1.2116
PE4	−1.2693	−0.8613	1.6844	0.2320							
PE5	0.2506	1.6917	1.4116	−1.2578							
PE6	−0.7805	−1.6895	1.5827	−2.6966							
n = 6											
MSE 0.00153											
PE1	0.6733	1.4579	0.8214	−0.1358	0.1363	−1.3047	0.7228	0.2202	−0.5337	1.1336	0.4762
PE2	−2.6351	0.4890	−1.9506	4.0996	−0.1619	−0.1563	−0.4588	0.4583	0.4437	−0.2361	−0.1789
PE3	−1.1670	0.9618	0.0373	0.1282	0.4459	0.0531	0.4703	0.3248	−0.0739	−0.2144	0.2003
PE4	1.6597	0.9956	−0.8489	0.1230							
PE5	3.5605	−1.6514	−0.6725	2.7244							
PE6	−.05519	−0.4616	3.4710	5.1559							

*PE = Processing elements.

References

[1] F.N. Alasfour, M.A. Darwish, A.O. Bin Amer, Thermal analysis of ME-TVC + MEE desalination system, Desalination 174 (2005) 39–61.

[2] R.K. Kamali, A. Abbassi, S.A. SadoughVanini, A simulation model and parametric study of MED-TVC process, Desalination 235 (2009) 340–351.

[3] M. Shakouri, H. Ghadamian, R. Sheikholeslami, Optimal model for multi effect desalination system integrated with gas turbine, Desalination 260 (2010) 254–263.

[4] M.A. Sharaf, A.S. Nafey, L. Garcia-Rodriguez, Thermo-economic analysis of solar thermal power cycles assisted MED-VC (multi effect distillation-vapor compression) desalination processes, Energy 36 (2011) 2753–2764.

[5] A.O. Bin Amer, Development and optimization of ME-TVC desalination system, Desalination 249 (2009) 1315–1331.

[6] H. El-Dessouky, H.M. Ettouney, F. Mandani, Performance of parallel feed multi effect evaporation system for seawater desalination, Appl. Therm. Eng. 20 (2000) 1679–1706.

[7] D. Zhao, J. Xue, S. Li, H. Sun, Q.D. Zhang, Theoretical analyses thermal and economical aspects of multi-effect distillation desalination dealing with high salinity wastewater, Desalination 273 (2011) 292–298.

[8] M. Al-Salahi, H. Ettouney, Developments in thermal desalination processes: design, energy and costing aspects, Desalination 214 (2007) 227–240.

[9] N. Lukic, L.L. Diezel, A.P. Froba, A. Leipertz, Economical aspects of the improvement of a mechanical vapour compression desalination plant by dropwise condensation, Desalination 264 (2010) 173–178.

[10] H.S. Choi, T.J. Lee, Y.G. Kim, S.L. Song, Performance improvement of multiple effect distiller with thermal vapor compression system by exergy analysis, Desalination 182 (2005) 239–249.

[11] K. Ansari, H. Sayyaadi, M. Amidpour, Thermoeconomic optimization of a hybrid pressurized water reactor (PWR) power plant coupled to a multi effect distillation desalination system with thermo-vapor compressor (MED-TVC), Energy 35 (2010) 1981–1996.

[12] M.A. Sharaf, A.S. Nafey, L. Garcia Rodriguez, Exergy and thermo-economic analyses of a combined solar organic cycle with multieffect distillation (MED) desalination process, Desalination 272 (2011) 135–147.

[13] I. Mohanty, D. Bhattacharjee, S. Datta, Designing cold rolled IF steel with optimized tensile properties, Comput. Mater. Sci. 50 (2011) 2331–2337.

[14] S. Wang, X. Dong, R. Sun, Predicting saturates of sour vacuum gas oil using artificial neural networks and genetic algorithm, Expert Syst. Appl. 37 (2010) 4768–4771.

[15] F. Vince, F. Marechal, E. Aoustin, P. Breant, Multi-objective optimization of RO desalination plants, Desalination 222 (2008) 96–118.

[16] C. Guria, P.K. Bhattacharya, S.K. Gupta, Multi-objective optimization of reverse osmosis desalination units using different adaptations of the non-dominated sorting genetic algorithm (NSGA), Comput. Chem. Eng. 29 (2005) 1977-1955.

[17] M.H. KhoshgoftarManesh, M. Amidpour, Multi-objective thermoeconomic optimization of coupling MSF desalination with PWR nuclear power plant through evolutionary algorithms, Desalination 249 (2009) 1332–1344.

[18] H. Sayyaadi, A. Saffari, A. Mahmoodian, Various approaches in optimization of multi effects distillation desalination systems using a hybrid meta-heusistic optimization tool, Desalination 254 (2010) 138–148.

[19] Y. Sun, W.D. Zeng, Y.F. Han, X. Ma, Y.Q. Zhao, Optimization of chemical composition for TC11 titanium alloy based on artificial neural network and genetic algorithm, Comput. Mater. Sci. 50 (2011) 1064–1069.
[20] M. Khayet, C. Cojocaru, M. Essalhi, Artificial neural network modeling and response methodology of desalination by reverse osmosis, J. Membr. Sci. 368 (2011) 202–214.
[21] M.E. Kazemian, A. Behzadmehr, S.M.H. Sarvari, Thermodynamic optimization of multi-effect desalination plant using the DoE method, Desalination (2010).
[22] K. Yetilmezsoy, S. Demirel, R.J. Vanderbei, Response surface modeling of pb(II) removal from aqueous by *Pistacia vera* L.: Box–Behnken experimental design, J. Hazard. Mater. 171 (2009) 551–562.
[23] M.A. Bezerra, R.E. Santelli, E.P. Oliveria, L.S. Villar, L.A. Escaleria, Response surface methodology (RSM) as a tool for optimization in analytical chemistry, Talanta 76 (2008) 965–977.
[24] F. Ghorbani, H. Younesi, S.M. Ghasempuri, A.A. Zinatizadeh, M. Amini, A. Daneshi, Application of response surface methodology for optimization of cadmium biosorption in an aqueous solution by *Saccharomyces cerevisiae*, Chem. Eng. J. 145 (2008) 267–275 Amsterdam, Neth.
[25] S. Wold, J. Trygg, A. Berglund, H. Antti, Some recent developments in PLS modeling, Chemom. Intell. Lab. Syst. 58 (2001) 131–150.
[26] S.J. Qin, Recursive PLS algorithm for adaptive data modeling, Comput. Chem. Eng. 22 (1998) 503–514.
[27] M.J. Lee, Y.S. Kim, C.K. Yoo, J.H. Song, S.J. Hwang, Sewage sludge reduction and system optimization in a catalytic ozonation process, Environ. Technol. 31 (2010) 7–14.
[28] Y. Sun, W. Zeng, X. Ma, B. Xu, X. Liang, J. Zhang, A hybrid approach for processing parameters optimization of Ti–22Al–25Nb alloy during hot deformation using artificial neural network and genetic algorithm, Intermetallics 19 (2011) 1014–1019.
[29] M.S. Bhatti, D. Kapoor, R.K. Kalia, A.S. Reddy, A.K. Thukral, RSM and ANN modeling for elecrocoagulation of copper from simulated wastewater: multi objective optimization using genetic algorithm approach, Desalination 274 (2011) 74–80.
[30] E.S. Elmolla, M. Chaudhuri, M.M. Hltoukhy, The use of artificial neural network (ANN) for modeling of COD removal from antibiotic aqueous solution by the Fenton process, J. Hazard. Mater. 179 (2010) 127–134.
[31] T. Nazghelichi, M. Aghbashlo, M.H. Kianmehr, Optimization of an artificial network topology using coupled response surface methodology and genetic algorithm for fluidized bed drying, Comput. Electron. Agric. 75 (2011) 84–91.
[32] H. Abu Qdais, K. Bani Hani, N. Shatnawi, Modeling and optimization of biogas production from a waste digester using artificial neural network and genetic algorithm, Resour. Conserv. Recycl. 54 (2010) 359–363.
[33] S. Aber, A.R. AminiGhadim, V. Mirzajani, Removal of Cr(VI) from polluted solutions by electrocoagulation: modeling of experimental results using artificial neural network, J. Hazard. Mater. 171 (2009) 484–490.
[34] A. Konak, D.W. Coit, A.E. Smith, Multi-objective optimization using genetic algorithm: a tutorial, Reliab. Eng. Syst. Saf. 91 (2006) 992–1007.
[35] N.K. Saxena, A. Khan, P.K.S. Pourush, N. Kumar, GA optimization of cutoff frequency of magnetically biased microstrip circular patch antenna, Int. J. Electron. (AEU) 65 (2011) 476–479.
[36] H.C. Liao, Using GA to dispatch the obtaining quantity for minimizing the total cost based on consideration of patient safety in HSCM, Expert Syst. Appl. 36 (2009) 11358–11362.
[37] M. Rajendra, P. Chandra Jena, H. Raheman, Prediction of optimization pretreatment process parameters for biodiesel production using ANN and GA, Fuel 88 (2009) 868–875.
[38] B. Sankararao, K. Santosh, Gupta, Multi-objective optimization of an industrial fluidized-bed catalytic cracking unit (FCCU) using two jumping gene adaptations of simulated annealing, Comput. Chem. Eng. 31 (2007) 1496–1515.